The distinct impacts of the two types of ENSO on rainfall variability over Southeast Asia

Hue Nguyen-Thanh, Thanh Ngo-Duc, Marine Herrmann

The distinct impacts of the two types of ENSO on rainfall variability over Southeast Asia

Authors: Hue Nguyen-Thanh[1,2], Thanh Ngo-Duc[1,*], Marine Herrmann[1,2]

1 - LOTUS Laboratory, University of Science and Technology of Hanoi (USTH), Vietnam Academy of Science and Technology (VAST), Vietnam

2 - Université de Toulouse, LEGOS, IRD/CNRS/CNES/UPS, Toulouse, France

Corresponding author: Thanh Ngo-Duc, ngo-duc.thanh@usth.edu.vn

ORCID: Thanh Ngo-Duc 0000-0003-1444-7498

Marine Herrmann 0000-0001-6125-7238

Hue Nguyen-Thanh 0000-0002-4834-9709

Accepted in Climate Dynamics : Nguyen-Thanh, H., Ngo-Duc, T. & Herrmann, M. (2023). The distinct impacts of the two types of ENSO on rainfall variability over Southeast Asia. *Clim Dyn* **61**, 2155–2172

https://doi.org/10.1007/s00382-023-06673-2

Acknowledgments

This work is supported by the LOTUS international joint laboratory (lotus.usth.edu.vn) funded by IRD, and the Vietnam National Foundation for Science and Technology Development (NAFOSTED). Hue Nguyen-Thanh's Ph.D. thesis is supported by the French Embassy in Vietnam via the scholarship of Excellence.

Abstract

This study investigates the impact of El Niño Southern Oscillation (ENSO) and ENSO Modoki on rainfall variability over Southeast Asia (SEA) with a focus on its twenty sub-regions. For the period 1979–2019, seven El Niño (EN), six La Niña (LN), five El Niño Modoki (EM), and five La Niña Modoki (LM) events were identified. In the boreal summer (JJA) and winter (DJF) of EN events, rainfall reduction occurred over the Maritime Continent and the Philippines except for West Philippines in JJA and West Kalimantan in DJF. Similar patterns but with enhanced drier/wetter conditions were detected during EM. During LN, rainfall increased in most sub-regions except for West Philippines and parts of mainland Indochina in JJA, and in DJF in some southern areas such as South Sumatra, West Kalimantan, and Papua. Compared to LN, LM generally exhibited less wet/drier conditions in JJA over most sub-regions and wetter conditions in DJF over a major part of the Maritime Continent. The decrease (increase) in rainfall over SEA during Modoki events compared to the canonical ENSO events was explained by a reduced (enhanced) moisture transport into the region and a weakening (strengthening) of the ascending branch of the Walker circulation.

Keywords: *ENSO, ENSO Modoki, rainfall variability, Southeast Asia*

1 Introduction

The El Niño Southern Oscillation (ENSO) is one of the most important climate phenomena that affect temperature and precipitation patterns across the globe via atmospheric teleconnections (Trenberth et al. 1998; Deser et al. 2017; Timmermann et al. 2018). Many studies focused on ENSO to predict its onset or investigate its impacts on weather and climate (Wang et al. 2011; Yan et al. 2020; Huang and Xie 2015). More recently, a new type of tropical Pacific Sea surface temperature (SST) warming pattern, with maximum warm anomalies in the central equatorial Pacific and cooler conditions in the eastern and western parts, has been discussed widely (Ashok et al. 2007; Weng et al. 2007; Marathe et al. 2015). This phenomenon is different from the canonical El Niño, which refers to anomalous warmings in the eastern equatorial Pacific (Rasmusson and Carpenter 1983). The new type of SST warming patterns was alternatively referred to as dateline El Niño (Larkin and Harrison 2005), central Pacific El Niño (Kao and Yu 2009), warm pool El Niño (Kug et al. 2009), or El Niño Modoki (Ashok et al. 2007; Weng et al. 2007, 2009). The opposite phase, with a cold sea surface temperature anomaly (SSTA) occurring in the central equatorial Pacific and warm SSTA in the eastern and western parts, is called La Niña Modoki (Ashok et al. 2007; Shinoda et al. 2011). Hereinafter, we use the term El Niño Modoki (EM) and La Niña Modoki (LM) for the new types of SST warming and cooling patterns to differentiate them from the canonical El Niño (EN) and La Niña (LN). EN and EM have different impacts on the spatial patterns of atmospheric and ocean variables (Kug et al. 2009). Those different impacts, particularly on precipitation, were investigated in numerous previous studies. EN events are in general associated with a reduction of rainfall over the western Pacific from the Philippines to West Australia, while a large area from the center to the eastern Pacific receives excess rainfall (Trenberth et al. 1998; McPhaden et al. 2006). Indeed, Ashok (2007) showed that during EM winters, the eastern Pacific experienced below-average rainfall. Moreover, the Philippines, South Thailand, and South India, along with some parts of North India, Sri Lanka, and East Africa, experienced abnormally dry conditions, whereas New Zealand, Pakistan, and Kazakhstan received excess rainfall.

Southeast Asia (SEA) comprises islands and the mainland of eleven countries: Cambodia, Laos, Vietnam, Thailand, Brunei, Philippines, Myanmar, Timor-Leste, Indonesia, Singapore, and Malaysia (Fig. 1). It has a tropical marine climate with high temperatures and abundant precipitation and is affected by monsoons (Räsänen et al. 2016; Tangang et al. 2020). Both rainfall and temperature display strong seasonality over most of SEA (Juneng and Tangang 2005; Phan et al. 2009; Juneng et al. 2016; Cruz et al. 2017; Alsepan and Minobe 2020). The rainfall season in the northern part of SEA, i.e. the Indochina peninsula and West Philippines, occurs mostly in the boreal summer (Matsumoto 1997; Francisco et al. 2006; Juneng et al. 2016; Tangang et al. 2020) while it mainly occurs in the boreal winter in the southern part and some specific locations of SEA, such as the Maritime Continent and East Philippines (Aldrian and Susanto 2003; Juneng et al. 2007; Juneng et al. 2016). The rainfall variations in SEA depend strongly on ENSO (Page et al. 2002; Wang et al. 2000; Hendon 2003; Wu et al. 2003; Juneng and Tangang 2005; Nguyen-Thi et al. 2012; Alsepan and Minobe 2020).

To date, the impact of ENSO Modoki on rainfall in SEA has not been fully addressed. Feng et al. (2010) studied the impact of EM on boreal winter rainfall in SEA for the period 1979–2008 using a coarse resolution dataset of 2.5º. They showed a negative rainfall anomaly during EM; however, the coarse resolution dataset they used did not allow an adequate representation of the heterogeneity of the rainfall pattern over the region. Salimun et al. (2013) also indicated the boreal winter rainfall deficit during EM, but their study domain was limited to Malaysia and the period 1950–2009. Alsepan and Minobe (2020) showed that EM conversely increases precipitation in West Indonesia in the wet season (November–April) compared to EN, but again, their study was limited to Indonesia and the period 1960–2007. The above studies moreover focused only on the impact of EM and not of LM. Feng et al. (2010) and Salimun et al. (2013) analyzed rainfall during boreal winter only. Last, the impact on rainfall during boreal summer has only been studied for the surrounding regions of SEA such as South China (Karori et al. 2013) and/or the Pacific rim (Weng et al. 2007) and not for the entire SEA region.

Besides the gaps highlighted above, more up-to-date datasets are now available, motivating the need to revisit or newly assess the impacts of ENSO and ENSO Modoki on rainfall variability over this landmass and its sub-regions. Moreover, we aim to explore the role of associated circulation conditions for the two types of ENSO in both boreal summer and winter months based on up-to-date reanalysis datasets. To sum up, our aim in this study is to use up-to-date datasets to assess the impacts of ENSO and ENSO Modoki on rainfall variability over SEA and all its sub-regions. We focus particularly on the distinct impacts of Modoki events compared with conventional ENSO and on the associated circulation mechanisms. This paper is composed of four sections. The study domain, datasets, and methods of analysis are described in section 2. We analyze our results in Section 3, where we examine with the most recent available data the impact of ENSO/ENSO Modoki on rainfall variability in different SEA sub-regions over a 41-year period (1979–2019). Section 4 investigates possible physical mechanisms responsible for the rainfall variations over the region. Conclusions are presented in Section 5.

2 Study domain, data, and method

2.1 Study domain

Figure 1 displays the SEA study domain and its 20 sub-regions defined by Juneng et al. (2016) under the framework of the Southeast Asia Regional Climate Downscaling/Coordinated Regional Climate Downscaling Experiment- Southeast Asia (SEACLID/CORDEX-SEA) project (Tangang et al. 2020). These 20 sub-regions were identified based on previous studies focusing on rainfall characteristics in SEA (Aldrian and Susanto 2003; Juneng and Tangang 2005; Francisco et al. 2006; Juneng et al. 2007; Chokngamwong and Chiu 2008; Nguyen-Thi et al. 2012; Salimun et al. 2013). In the following, the impacts of the two types of ENSO on rainfall will be examined over the whole SEA area as well as over these sub-regions.

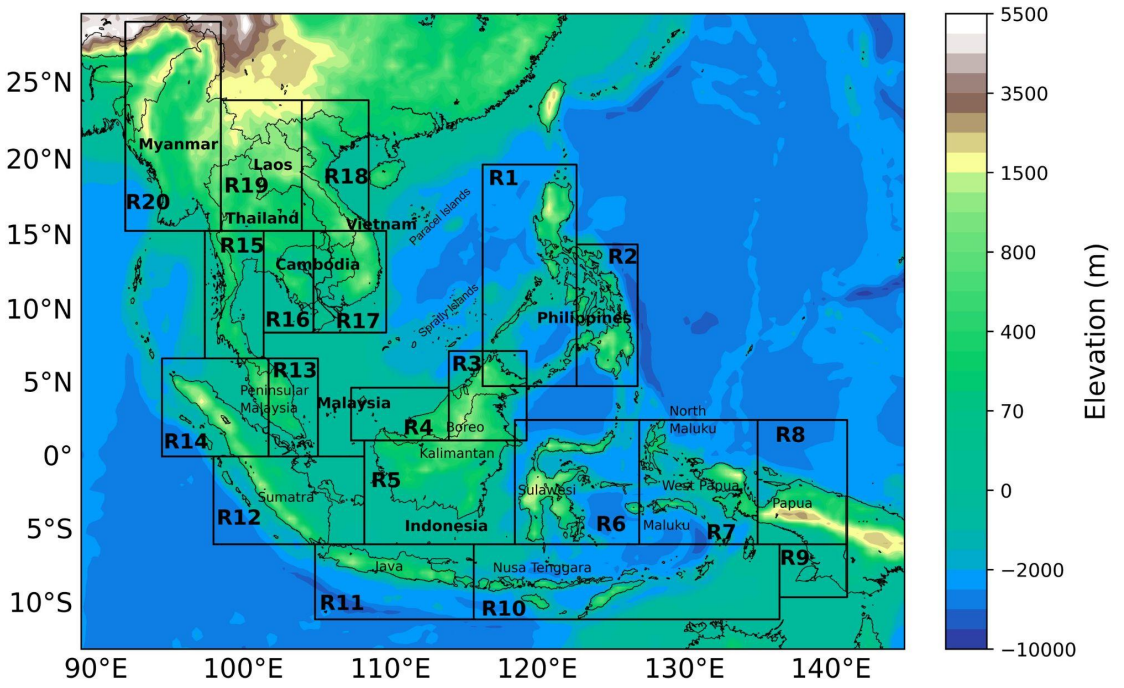

Figure 1. The Southeast Asia domain and its 20 sub-regions used for the assessment (delineated by black boxes). Topography over SEA (shaded) is obtained from the Global 30 Arc-Second Elevation (GTOPO30) data set.

2.2 Data

To identify ENSO and ENSO Modoki months, we used monthly SST data from the Hadley Centre Global Sea Ice and Sea Surface Temperature (HadISST) (Rayner et al. 2003). This dataset has a spatial resolution of 1°×1° and covers the period 1979–2019.

The rainfall dataset is obtained from the Global Precipitation Climatology Centre (GPCC) version 2020 (Rudolf et al. 1994). Here we used the monthly land dataset for the period 1979–2019 at a resolution of 0.25º × 0.25º.

To analyze the possible physical mechanisms explaining the impacts of the two types of ENSO on rainfall in SEA, the European Center for Medium-Range Weather Forecasts (ECMWF) Reanalysis version 5 (ERA5) dataset (Hersbach et al. 2020) was used. The ERA5 data used in this study has a horizontal resolution of 0.25º×0.25º. The variables include specific humidity (q), meridional wind (v), zonal wind (u), and vertical

velocity (omega), which are provided on 23 pressure levels between 1000 hPa and 200 hPa, and the vertical integral of moisture flux divergence (div).

Furthermore, to examine the sensibility of the obtained results to the choice of datasets, we also perform the analysis with other rainfall and reanalysis datasets, including the Climate Research Unit (CRU) rainfall data (version TS v. 4.05; Harris et al. 2020), and the National Centers for Environmental Prediction (NCEP)/National Center for Atmospheric Research (NCAR) Reanalysis-1 (hereafter called NCEP1; Kalnay et al. 1996) data. The horizontal resolutions of the CRU and NCEP1 are 0.5º×0.5º and 2.0º×2.0º, respectively. They all cover the study period 1979–2019.

2.3 Method

In this study, an EN (LN) event is identified when the normalized 3-month running mean of the SST anomalies (SSTAs) in the Niño3 region (5°S–5°N, 150°W–90°W; Fig. 2a) exceeds 0.5ºC (is lower than -0.5ºC) for at least five consecutive months, as implemented in previous studies (e.g. Trenberth 1997; Yeh et al. 2009; Shukla et al. 2011). An ENSO event usually begins in boreal summer, peaks in boreal winter, and decays in the following spring (Rasmusons and Carpenter 1982; An and Wang 2001; Chen and Jin 2020). For a year (denoted as Year0) where an EN or LN event is detected in the boreal winter months, the seasonal rainfall averages of that ENSO event are thus computed for four seasons: June-July-August (JJA) of YEAR0, September-October-November (SON) of YEAR0, December-January-February (DJF) with December of YEAR0 and January-February of the following year (denoted as YEAR+1), and March-April-May (MAM) of YEAR+1.

To identify ENSO Modoki events, we use the El Niño Modoki index (EMI) defined by Ashok et al. (2007) and used in previous studies (e.g. Weng et al. 2009; Yu et al. 2012, 2013):

$$EMI = [SSTA]_A - 0.5\times[SSTA]_B - 0.5\times[SSTA]_C \quad (1)$$

Brackets in Equation (1) represent the area average over the central Pacific region A (10°S–10°N, 165°E–140°W), the Eastern Pacific region B (15°S–5°N, 110°–70°W), and the Western Pacific region C (10°S–20°N, 125°–145°E), as shown in Fig. 2b. An EM (LM) event is identified when the normalized 3-month running mean of the EMI is larger than 0.7×σ (smaller than -0.7×σ), where σ is the standard deviation of the EMI, for at least five consecutive months. Similar to ENSO, for a year where an EM or LM event is detected in the boreal winter months, the seasonal rainfall averages of that ENSO Modoki event are computed for the four seasons JJA, SON, DJF, and MAM.

Previous studies for the SEA region focused on the EM impacts on DJF rainfall (Feng et al. 2010; Salimun et al. 2013). In this study, we analyze the ENSO and ENSO Modoki impacts on rainfall in both DJF and JJA, which are mainly the rainy seasons over the southeastern part (subregions R2–14 shown in Fig. 1) and the northern part (subregions R1, R15–20) of SEA, respectively. To avoid repetitive texts and figures, the impacts on SON and MAM rainfall are displayed in supplemental figures (SFig. 2, SFig. 3).

To quantify the impact of the two types of ENSO on seasonal rainfall, e.g. the impact of EM on DJF rainfall, we compute the difference between the average of DJF rainfall for all EM years (5 years, see Table 1) and the average of DJF rainfall for all neutral years (16 years, see Table 1). For simplicity, the term "anomaly" used in the text corresponds to this difference. Previous studies did not compute the DJF rainfall of the neutral years but computed the climatological DJF rainfall, i.e. the average DJF rainfall for the whole study period. The drawback of using the climatological values is that they might be influenced by the dominant signal of one of the four ENSO or ENSO Modoki modes, which was the most active during the study period. Indeed, over the study period of 1979–2019, the difference between the neutral values and the climatological values of rainfall (SFig.1) displays similar patterns as the difference between the EN/EM values and the neutral values, particularly in DJF over the whole domain and in JJA over the Indochinese Peninsula (cf. Fig. 4). Moreover, with the choice of neutral years, we can estimate the significant level of the impacts by using the

bootstrapping technique detailed by Efron and Tibshirani (1993). 1000 bootstrap replications of size n_{EM}=5 (n_{EN}=7, n_{LM}=5, n_{LN}=6, see Table 1) and $n_{neutral\ years}$=16 are generated to estimate the difference between EM (EN, LM, LN) and the neutral years.

To analyze the possible physical mechanisms associated with the two types of ENSO, the vertically integrated moisture flux (VIMF) and velocity potential were estimated based on monthly mean values computed from the reanalysis dataset.

The VIMF $\overrightarrow{Q}$ (units: kg m^{-1} s^{-1}) was calculated by:

$$\vec{Q} = -\frac{1}{g}\int_{p_s}^{p_t} \overrightarrow{qV}\, dp \qquad (2)$$

where g is the gravity acceleration (9.8 m s^{-2}), q the specific humidity, $\overrightarrow{V}$ the horizontal wind vector, p_s the surface pressure, and p_t the pressure at the top of the atmosphere. Since most of the water vapor in the atmosphere is located below 200 hPa (Li et al. 2011) and the specific humidity above 200 hPa has a minimal effect on the VIMF (Kalnay et al. 1996; Fasullo and Webster 2003), the VIMF in this study was calculated with the pressure data from the surface to the 200 hPa level. We have also computed the VIMF for the whole atmospheric column by integrating the data from the surface to the 01 hPa level and obtained almost identical results with those below the 200 hPa level (not shown).

The potential velocity scalars were estimated by decomposing the horizontal wind into the rotational and divergent components according to the Helmholtz theorem (Helmholtz 1867). Finally, vertical velocity (omega) from 1000 to 200 hPa were used to describe the intensity and spatial extent of the convection processes in the region. Negative (positive) vertical velocity anomalies denote ascending (descending) vertical motion enhancements.

3 The two types of ENSO and associated rainfall variations during the period 1979–2019

3.1 EOF analysis

The purpose of this section is to re-examine the ENSO and ENSO Modoki patterns and identify the months in which those events occurred during the period 1979–2019 in order to confirm and update previous findings (e.g. Ashok et al. 2007) with more recent SST data.

An empirical orthogonal function (EOF) analysis was performed on the monthly mean SSTA over the domain of 100°E–80°W, 30°S–30°N to obtain the principal modes of SST variability over the tropical Pacific and to distinguish the two types of EN events. The first EOF mode (EOF1) corresponds to the EN pattern. It is characterized by a strong anomalous warming in the central-eastern equatorial Pacific and an anomalous cooling in the western tropical Pacific (Fig. 2a). This pattern, associated with its principal component (PC1, Fig. 2c), explains about 42% of the tropical Pacific SST variability for the study period 1979–2019. Similarly, Xu et al. (2017) and Bo and Ren (2019) found that 52% and 48% of the SST variability were explained by the EOF1 for the periods 1950–1999 and 1979–2016, respectively. The correlations between the PC1 and the Niño3, Niño3.4, and Niño4 indices reach highly significant values of 0.97, 0.96, and 0.93, respectively (Fig. 2).

The second EOF (EOF2), with an explained variance of 11%, is characterized by a zonal tripole pattern with warmer-than-normal SST in the central equatorial Pacific and colder SST in the eastern and western tropical Pacific (Fig. 2b). It corresponds to the EM patterns. Similarly, Ashok et al. (2007) and Bo and Ren (2019) found that 12% and 11% of the SST variability were explained by the EOF2 for the period 1979–2004 and 1979–2016, respectively. The slight difference between those studies can be attributed to the differences in the analysis periods or the SST data used. The EOF2 of the SSTA pattern, associated with the positive phase of its principal component (PC2, Fig. 2d), is consistent with the EM pattern previously identified (Ashok et al. 2007; Yu

and Kao 2007). The PC2 series correlates well with the EMI, with a correlation value of 0.78 (Fig. 2).

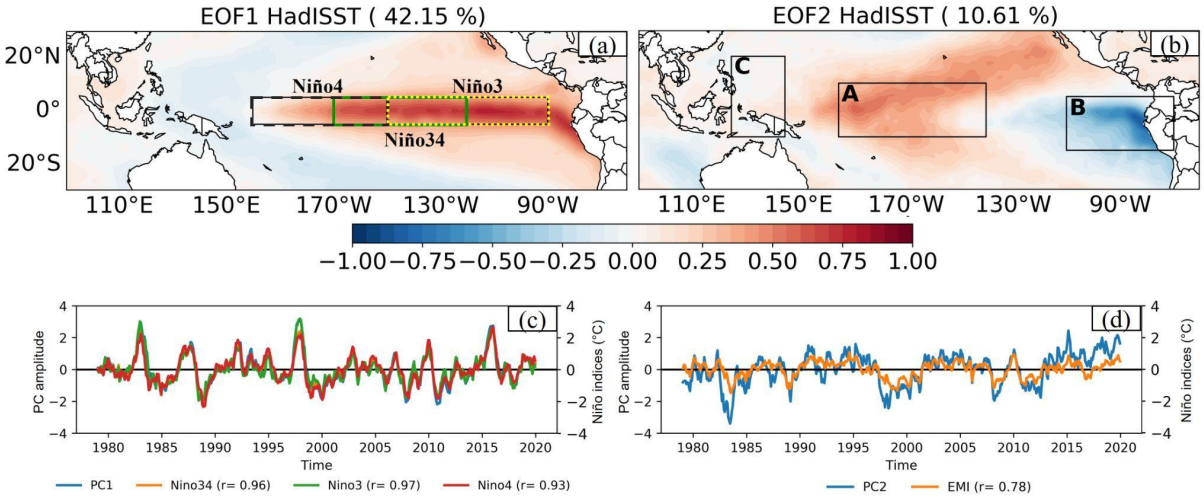

Figure 2. EOF patterns of the HadISST anomalies (1979–2019) for (a) the 1st mode, corresponding to a typical EN, (b) the 2nd mode, corresponding to a typical EM; and time series of (c) the PC1 and Niño3, Niño3.4, and Niño4 indices, and (d) the PC2 and EMI. Locations of the Niño3 (5°S–5°N, 150°W–90°W), Niño3.4 (5°S–5°N, 170°W–120°W), and Niño4 (5°S–5°N, 160°E–150°W) regions are indicated in (a). Boxes A (10°S–10°N, 165°E–140°W), B (15°S–5°N, 110°–70°W), and C (10°S–20°N, 125°–145°E) in (b) are used for computing the EMI. The numbers in parentheses in (c) and (d) indicate the correlations between the corresponding indices with the PC1 and PC2 series, respectively.

The high correlations between the PC series and the Niño and EMI indices indicate that the first two modes of SSTA over the tropical Pacific, i.e. the ENSO and Modoki patterns, can be well represented by the Niño and EMI indices. Since the correlation between the PC1 and the Niño3 index reaches the highest value of 0.97, the Niño3 index is used in this study to identify canonical ENSO events. Nevertheless, it is worth mentioning that using the Niño3.4 index provides almost identical ENSO years except for the weak El Niño year 1987/1988 that was detected by the Niño3.4 index but not by the Niño3 index (Supplemental Table 1). There are also minor differences of +/- 1 month in the starting/ending time of some ENSO events if we use the Niño3.4 index instead of the Niño3. Note that the Niño4 region (5°S–5°N, 160°E–150°W) was not chosen for detecting ENSO events in this study because it is more in the central Pacific compared to the Niño3 and Niño3.4 regions, hence it could reflect variations of both

Modoki and canonical ENSO events (Weng et al. 2009). The correlations between the Niño4 index and the PC2 and the EMI are 0.21 and 0.60, respectively, reaching the highest values when compared with the results of the Niño3 and Niño3.4 indices.

Using the criteria defined in Section 2.c, seven EN, six LN events, five EM and five LM events were identified over the study period of 1979–2019 (Table 1). 16 years are classified as neutral years (Table 1). The ENSO events generally started in the fall (Supplemental Table 1). However, there were five early-onset events that started from April to June, including the two El Niño events of 04/1982–06/1983 and 05/1997–05/1998, and the three La Niña events of 04/1988–10/1988, 06/1999–03/2000, and 06/2010–05/2011. The timing of these events is confirmed by cross-checking with the historical ENSO episodes provided by the Climate Prediction Center (CPC) of the National Oceanic and Atmospheric Administration (NOAA) (NOAA-CPC, 2022).

Among the 16 neutral years in Table 1, 1979/1980 and 1990/1991 were classified as EM years in some previous studies (Feng et al. 2010; Salimun et al. 2013); 1987/1988 was classified as an EN year (Salimun et al. 2013). The differences between those studies and our study can be attributed to the different indices, dataset periods, or thresholds used to detect those three weak EN and EM events. We have conducted an additional analysis (not shown) that considers 1979/1980 and 1990/1991 as EM years and 1987/1988 as an EN year. This analysis confirms that the results shown in the following subsections stay robust regardless of the classification of those three years.

Table 1. List of EN, LN, EM, LM, and neutral years over the period of 1979–2019. The number in parentheses indicates the total number of years for each type of event.

EN (7)	LN (6)	EM (5)	LM (5)	Neutral (16)
1982/1983	1984/1985	1991/1992	1983/1984	1979/1980
1986/1987	1995/1996	1994/1995	1988/1989	1980/1981
1997/1998	1999/2000	2002/2003	1998/1999	1981/1982

2006/2007	2007/2008	2004/2005	2008/2009	1985/1986
2014/2015	2010/2011	2009/2010	2011/2012	1987/1988
2015/2016	2017/2018			1990/1991
2018/2019				1992/1993
				1993/1994
				1996/1997
				2000/2001
				2001/2002
				2003/2004
				2005/2006
				2012/2013
				2013/2014
				2016/2017

3.2 Rainfall variations in ENSO and ENSO Modoki events

a) Relationship between SST and rainfall over SEA

To examine and confirm the relationship between SST and rainfall over SEA, we compute the correlation coefficient between Niño-3 and EMI indices and monthly rainfall anomalies, using 3-months running averages of each dataset (Fig. 3). The annual cycle was removed from the time series before computing the correlations.

Figure 3a shows significant negative correlations between monthly rainfall anomalies and the Niño-3 index over all SEA subregions, with values varying from -0.5 to -0.2. In the areas of South Philippines (R2), East Borneo (R3), Maluku, and West

Papua (R7), the correlation between rainfall and the Niño-3 index reaches the largest value of -0.45, while it is positive in Southeast China (0.5). The negative correlation pattern implies that a warm (cold) SST in the Niño-3 region, corresponding to an EN (LN) phase, leads to a decrease (increase) in rainfall over SEA. Similar results were shown in the study of Hendrawan et al. (2019): an increase in SST leads to a decrease in rainfall over the Indonesian region (R5–12, R14). Harger (1995) also showed that EN events are generally associated with decreased rainfall over the Philippines and Indonesia.

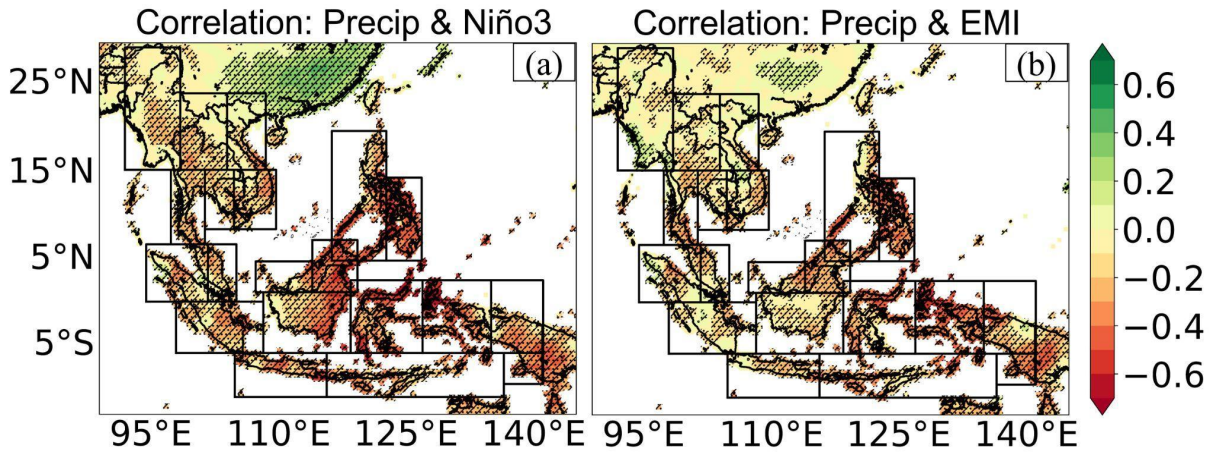

Figure 3. Spatial distribution of correlations between monthly rainfall anomalies and (a) the Niño-3 index and (b) the EMI. The dot pattern indicates areas where the correlations are statistically significant at 90% based on the Student's t-test.

The correlation coefficient between rainfall anomalies and the EMI is also negative in most of SEA, with absolute values usually less than 0.35 (Fig. 3b). Those correlations are weaker and less significant than correlations with Niño-3, and areas with correlation reaching statistical significance are also smaller. The correlation is insignificant in North Laos (R18–19), North Vietnam (R18), Myanmar (R20), and South Sumatra (R12). The correlation coefficient is significantly positive in the central part of the southeastern China region, while the remaining southern areas have small correlation values that do not reach the significance level ($|r|<0.2$). Overall, the correlation between the average rainfall over the entire SEA and the Niño-3 and the EMI is 0.66 and 0.60, respectively.

b) Rainfall anomaly patterns

Figure 4 displays the spatial distribution over the SEA domain of the JJA and DJF composites of rainfall anomalies for the EN and EM years and the differences between them, i.e. EM minus EN. Rainfall reduction occurs throughout most sub-regions from 5N southward (R3–13) and Southeast Philippines (R2) in JJA of EN events (Fig. 4a). Significant rainfall reduction of about 2–3.5 mm/day is observed over Kalimantan (R5), Maluku and West Papua (R7), Java (R11), and South Sumatra (R12). However, the EN impacts on JJA rainfall over the Indochinese Peninsula (R16–20) are not significant, with alternating drier and wetter conditions from -1 to 1 mm/day. In DJF of EN events, while larger rainfall reduction compared to JJA is seen over Southeast Philippines (R2), East Borneo (R3), and Maluku (R7), there is a significant rainfall enhancement of about 1–3 mm/day over West Kalimantan (R5) and part of the Indochinese Peninsula (R18–R20) (Fig. 4b). The rainfall reduction during EN identified here is in agreement with previous findings in the region, e.g. Salimun et al. (2013) for Peninsular Malaysia and North Borneo, and Juneng and Tangang (2005) for Southeast Asia. Besides, although the Southeast China region is outside the study area, it is noteworthy to mention that the rainfall increase (~1–2.5 mm/day) over this area during EN conditions is consistent with previous studies (Feng and Hu 2004; Xue and Liu 2008; Karori et al. 2013).

The general anomaly patterns of EM (Fig. 4c,d) are very similar to those of EN (Fig. 4a,b) for both JJA and DJF. However, the anomaly magnitudes are not the same (Fig. 4e,f). Generally, EM shows enhanced drier/wetter conditions compared to EN. In JJA, EM produces more rainfall than EN does in the eastern side of the domain and less rainfall in the southwestern part. The opposite is found in DJF, i.e. EM produces less rainfall than EN does in the eastern side and more rainfall in the southwestern part. In Section 4, we will discuss the mechanism of these systematic seasonal differences.

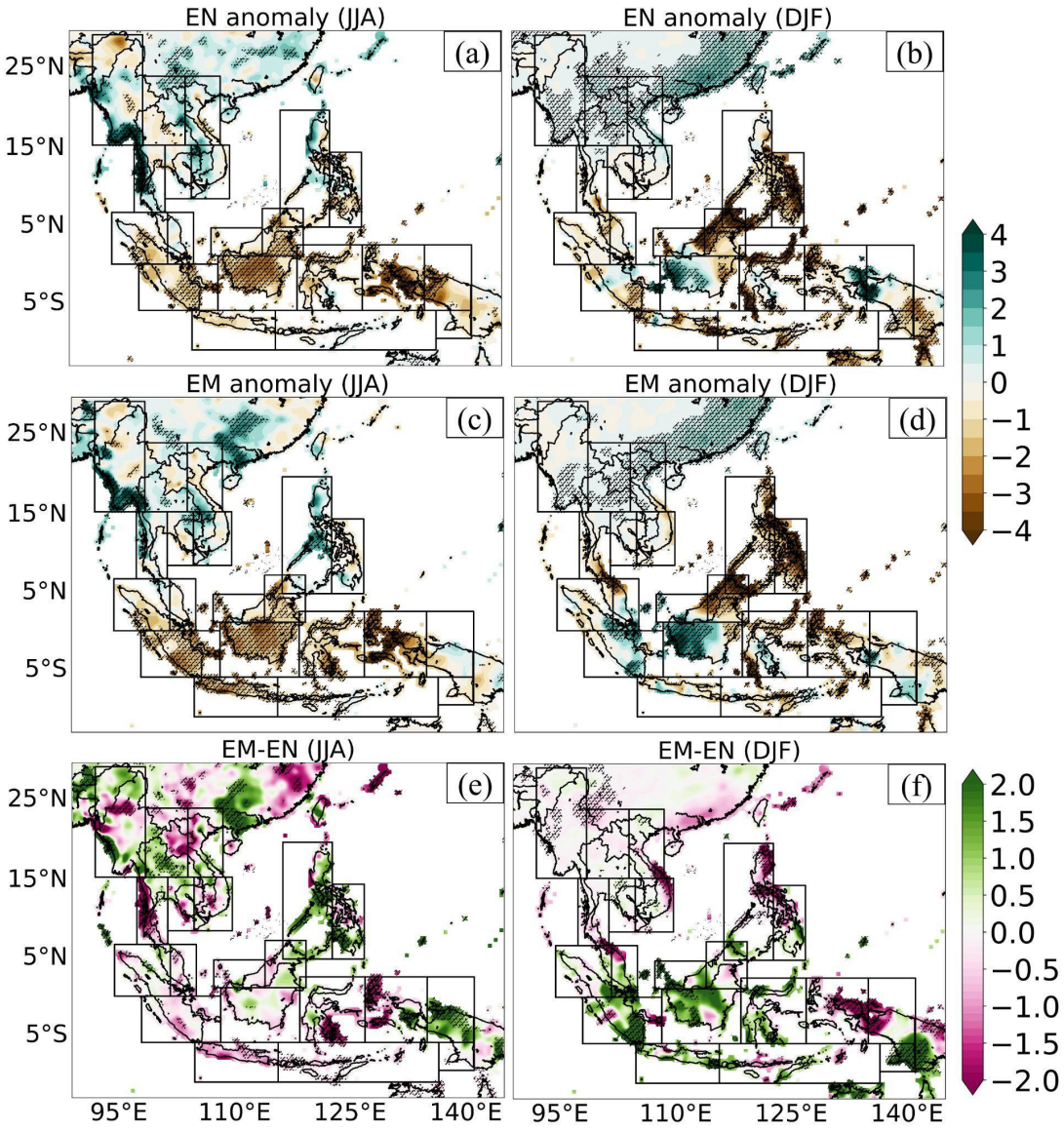

Figure 4. Composites of JJA and DJF rainfall anomalies (units: mm/day) for (a, b) EN, (c, d) EM, and (e, f) the differences between EN and EM. The dot pattern indicates areas where differences are statistically significant at 90% based on the bootstrap test.

Rainfall increase occurs throughout most sub-regions in JJA of LN events except for West Philippines and some specific locations in the Indochinese Peninsula where the rainfall reduction is usually not statistically significant (Fig. 5a). Significant rainfall increase of about 2–3.5 mm/day is observed during LN over Borneo (R4), Kalimantan (R5), Sulawesi (R6), and Maluku and West Papua (R7). Similar to EN, the LN impacts on JJA rainfall over the Indochinese Peninsula (R16–20) are not homogeneously

significant, with alternating drier and wetter conditions from -1 to 1 mm/day (Fig. 5a). In DJF of LN events, while larger rainfall compared to JJA is seen over southeastern Philippines (R2), there is a rainfall depletion of about 1–1.5 mm/day over some areas in the southern part of SEA, such as South Sumatra (R12), West Kalimantan (R5), and Papua (R8) (Fig. 5b). The rainfall increase over the western part of Indochina in the dry months DJF during LN is statistically significant although the increased amount is relatively small (less than 0.5 mm/day).

The main anomaly patterns of LM (Fig. 5c,d) are similar to those of LN (Fig. 5a,b). For JJA, LM also displays increased rainfall over the Maritime Continent and North Thailand, and reduced rainfall over West Philippines (Fig. 5c). For DJF, LM exhibits increased rainfall over the northern Maritime Continent and the Philippines, while showing alternating drier and wetter conditions over the Indochinese Peninsula and the southern rim of the SEA domain. Nevertheless, the anomaly magnitudes are not the same (Fig. 5e,f). In JJA, LM generally shows less wet/drier conditions than LN, particularly in Central Vietnam (R17–18) and the coastal regions of Myanmar (R15 and R20) (Fig. 5e). Some exceptions can be found over some specific locations such as Southeast Philippines (R2) and North Sumatra (R14) where LM produces more rainfall compared to LN. In DJF, compared to LN, LM exhibits more rainfall over a major part of the Maritime Continent while generally displaying less rainfall over Indochina (R15–20), Southeast Philippines (R2), and part of Sulawesi (R6).

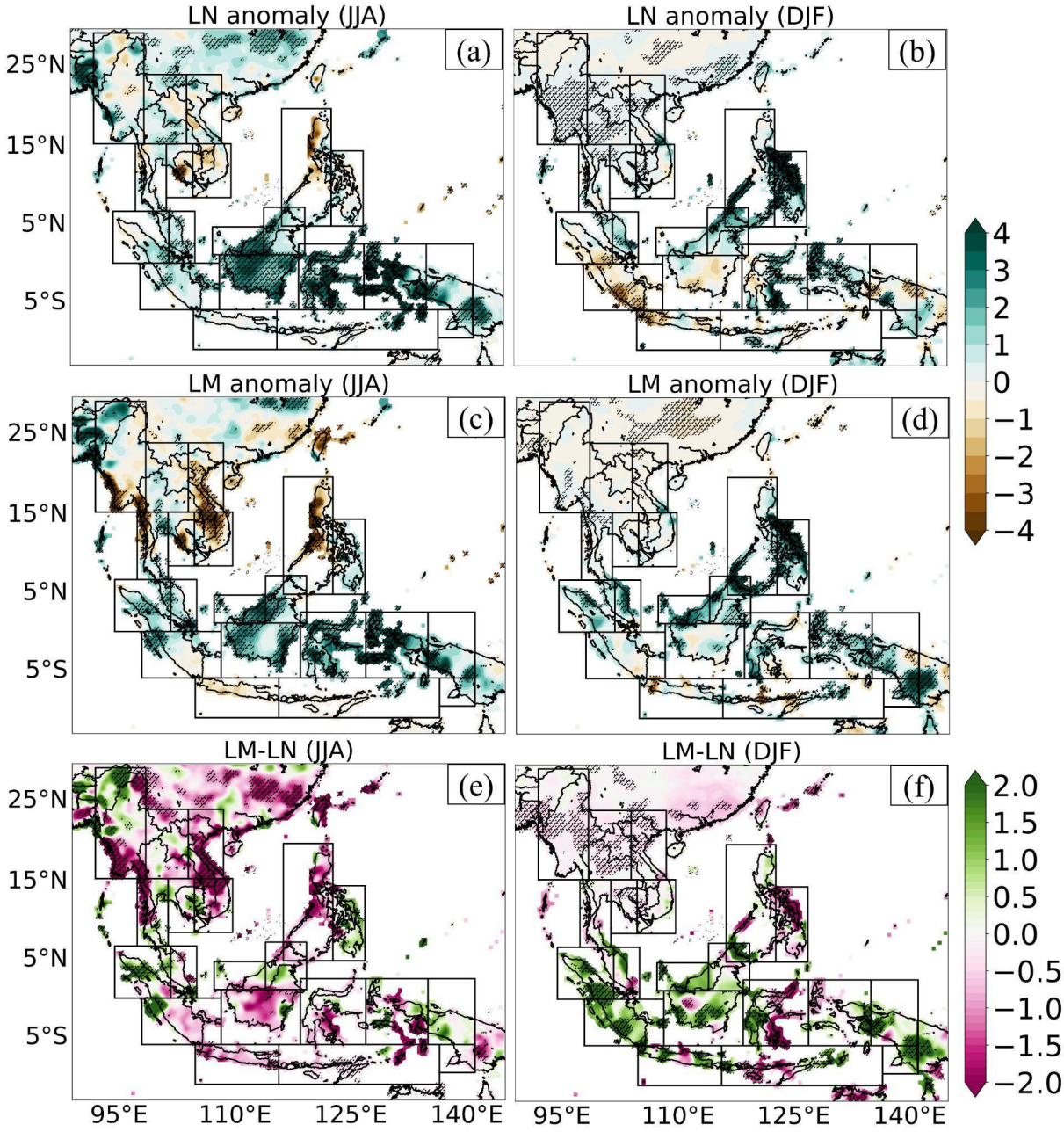

Figure 5. As in Fig. 4 but for LN and LM.

c) Rainfall anomaly averaged over the 20 SEA sub-regions

Figure 6 summarizes the detailed changes in rainfall over the 20 SEA sub-regions. As seen above, rainfall in JJA in the eastern rim of SEA (i.e. R1, R2, R8, and R18) is less reduced during EM compared to EN, while the remaining subregions generally experience more rainfall reduction during EM (Fig. 6a,b). In contrast, less rainfall in the eastern rim and more rainfall in the southern subregions (R4–6, R9–14) is

obtained in DJF of EM compared to EN. The highest rainfall deficit during EN occurs in R2–3 in DJF (~2.5 mm/day) and in R7 in JJA (~2 mm/day) and can lead to significant drought conditions over these areas (Saji et al. 1999; Webster et al. 1999; D'Arrigo and Smerdon 2008; Lestari et al. 2016). Droughts during EM are thus expected to be less severe than during EN in almost all subregions, except for some parts of Indonesia (R6–7, R10–R12) during JJA.

During LN, the largest rainfall increase occurs over the east of the Philippines (R2) in DJF and part of Indonesia (R5–7) in JJA, with a rainfall increase exceeding 2.5–3 mm/day on average (Fig. 5c,d). In JJA, LM shows drier characteristics than LN for almost all subregions as also indicated in Fig 4e. In DJF, LM generally exhibits more rainfall than LN over subregions R3–14, i.e. over the Maritime Continent. LN could induce severe floods in the region in DJF (Tangang et al 2017), that could thus be worsened in LM.

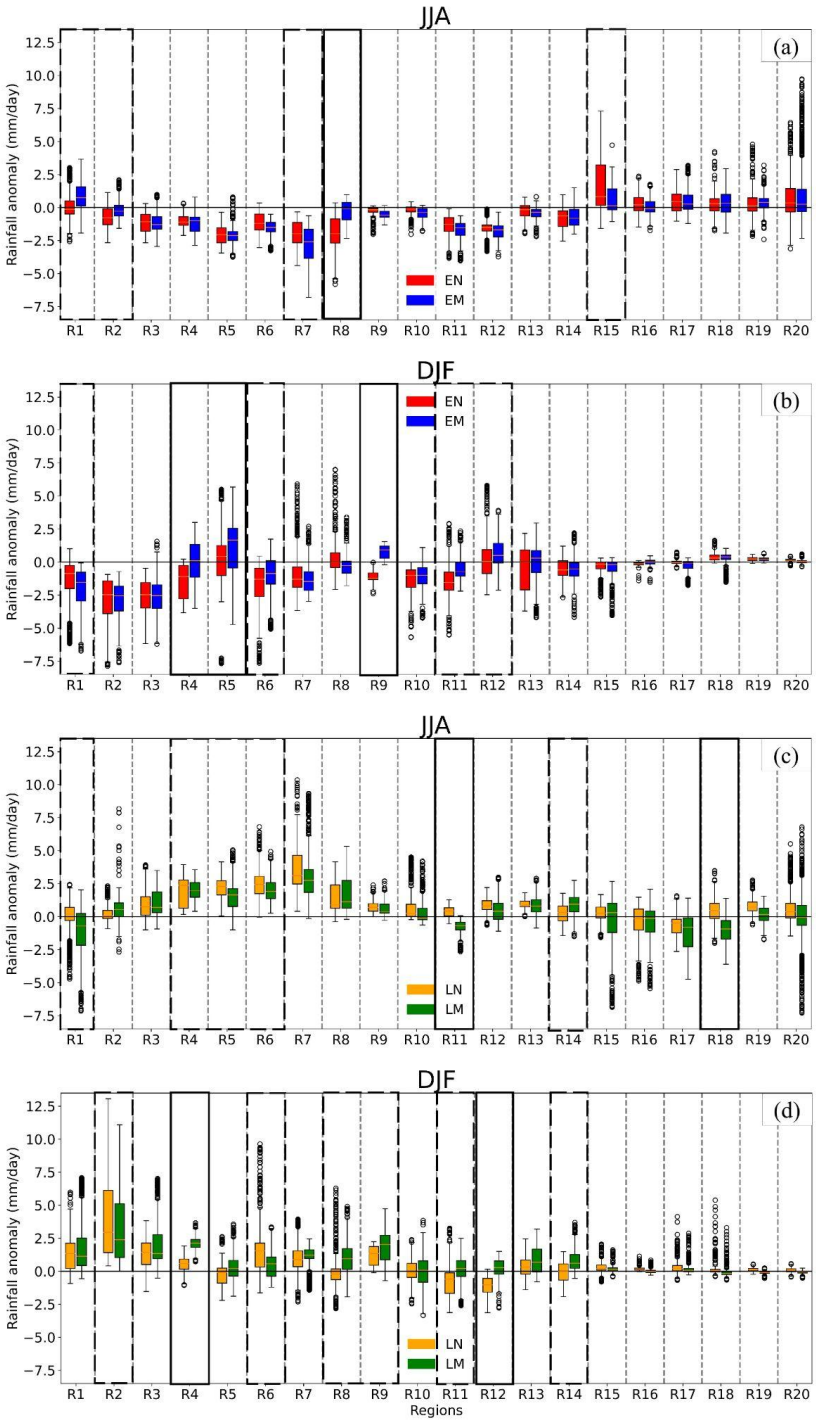

Figure 6. Box plots of average JJA and DJF rainfall anomaly over 20 sub-regions for (a,b) EN (red) and EM (blue), (c, d) LN (yellow) and LM (green). Units in mm/day. The subregions where the differences between EN and EM (and between LN and LM) mean values are within 0.5–1mm/day and above 1mm/day are highlighted in black dashed line and solid line boxes, respectively.

4 Possible mechanisms responsible for the rainfall variations

4.1 Vertically Integrated Moisture Flux

The transport direction and origins of VIMF are associated with rainfall anomaly patterns (Zhou and Yu 2005). The VIMF anomaly allows identifying the areas of divergence (positive values) and convergence (negative values) of the moisture fluxes that correspond to rainfall decrease or increase, respectively.

Figure 7a,b displays the VIMF and its divergence over the SEA domain for the neutral JJA and DJF composites. The wet conditions in JJA over the northern domain, i.e. Indochina and the Philippines, mainly originate from the moisture transport by the southwest monsoon from the Bay of Bengal in the Indian Ocean to the west of the domain, and by the Pacific easterlies to the east of the domain. Most of the Maritime Continent experiences dry conditions because of a lack of moisture supply to the region in JJA. In DJF, the SEA domain is well separated into a northern dry area and a southern wet area. The moisture transport to the Maritime Continent in DJF originates from the equatorial westerlies in the southern hemisphere, and from the Pacific easterlies in the northern hemisphere.

Figures 7c–f show both in EN and EM events a decrease in moisture transport from the Pacific in both JJA and DJF as well as from the equatorial easterlies in the southern hemisphere to parts of SEA in DJF. The moisture deficit in EM is larger (smaller) than that in EN over the Maritime Continent in JJA (DJF) (Fig. 7g,h). Anomalous divergent conditions (positive values in Fig. 7c–f) prevail noticeably over the Maritime Continent in JJA and the northern part of the Maritime Continent and the Philippines in DJF in both EN and EM, inducing an inhibition, i.e. deficit, of rainfall over these subregions. This is in agreement with the results discussed above and shown in Fig. 5a. In EN, weak anomalous convergences are observed in Southeast China, part of Indochina (R19, R20), and North Sumatra (R14) in both seasons, and South Borneo (R4) in DJF. Furthermore, relatively strong anomalous convergences in the coastal region of Myanmar (part of R15, R20) in JJA and West Sumatra (part of R12, R14) in

DJF are observed in EM, resulting in increased rainfall over this region. The anomalous convergence regions in EN and EM could be explained by enhanced moisture transport from the Bay of Bengal in JJA, e.g. in Indochina, or by the redistribution of the moisture budget within the regions in DJF, e.g. in Sumatra. Values corresponding to anomalous divergence (convergence) conditions in JJA (DJF) during EM are generally larger than those during EN over the Maritime Continent, causing and explaining the stronger rainfall decrease (increase) during EM than during EN in this region as shown in Fig. 4.

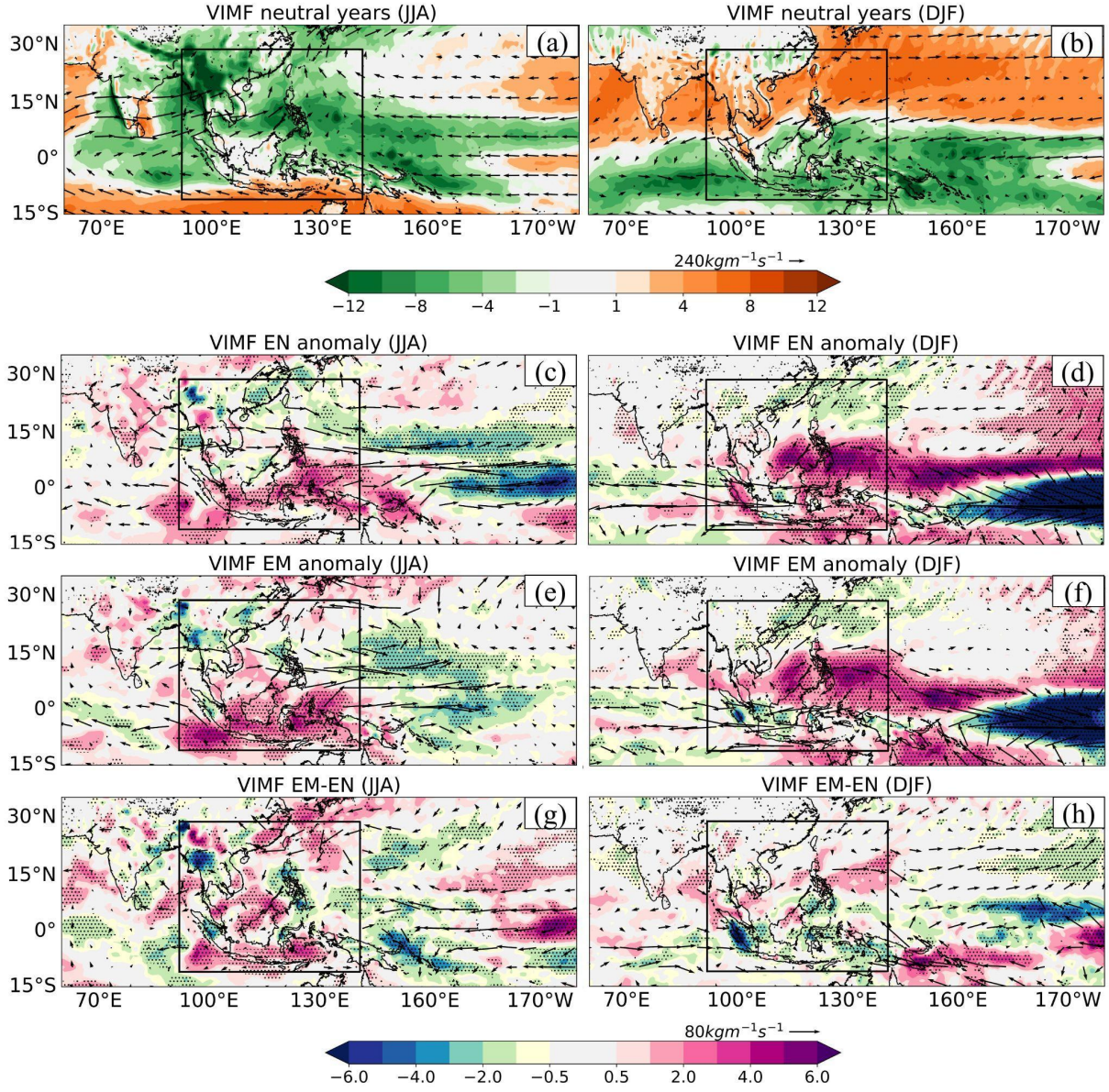

Figure 7. VIMF (vector, unit: kg $m^{-2}s^{-1}$) and its divergence (shading, unit 10^{-5} kg $m^{-2}s^{-1}$) for JJA and DJF of the neutral years (a, b), anomalies of the composites of EN (c, d) and EM (e, f) and differences

between EM and EN (g, h) during JJA and DJF. The dot patterns in (c–h) indicate areas where differences are statistically significant at 90% based on the bootstrap test.

Figure 8 displays the VIMF anomaly in LN and LM and the differences between LM and LN. Under LM conditions, moisture north of 10°N (from the Bay of Bengal and Northwest Pacific Ocean) is considerably reduced in JJA, mainly due to a deficit in the moisture transport by summer monsoon into the west, and by the Pacific easterlies into the northeast of the domain (Fig. 8c). On the other hand, moisture in LM increases over the southern SEA region (5ºN–15ºS, 100ºE–150ºE) in both JJA and DJF because of enhanced moisture transport into the east of the domain by the Pacific easterlies in both seasons, and into the west of the domain by the equatorial westerlies in DJF (Fig. 8c,d). As a result, rainfall in LM decreases sharply in JJA in the subregions from 10ºN northward such as Vietnam (R17, R18) and West Philippines (R1), and generally increases in the southern subregions in both seasons (Fig. 5c,d). The VIMF anomaly, as well as its anomalous divergence/convergence conditions, show similar patterns under LN with some differences in magnitude compared to LM. In JJA, LN exhibits less reduced (more enhanced) moisture transport than LM over the northern (southern) subregions (Fig. 8e), leading to less rainfall over these subregions, respectively (cf. Fig. 5e). In DJF, LM shows enhanced convergence compared to LN in most of the southern subregions (Fig. 8f), explaining the rainfall enhancement over these regions during LM (cf. Fig. 5f).

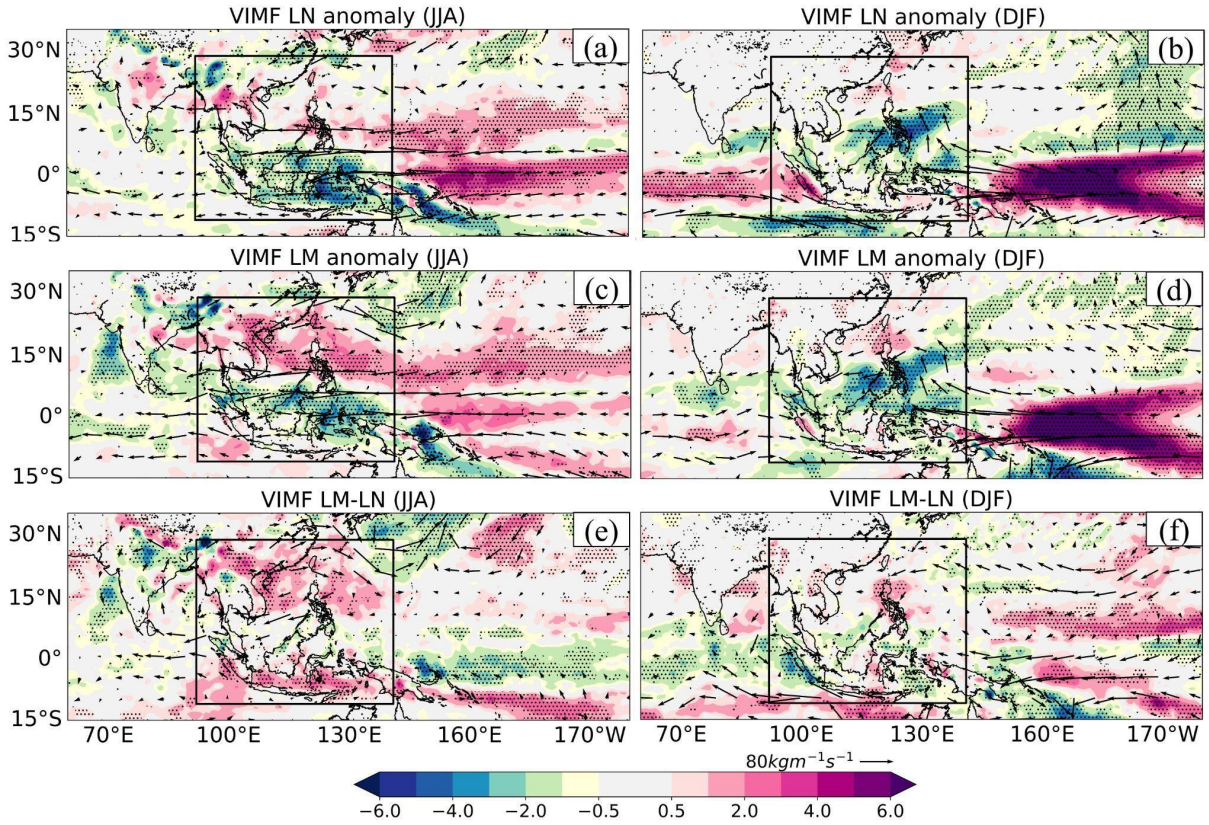

Figure 8. As in Fig. 7(c–h) but for LN and LM.

4.2 Associated circulation cells

For the identification of atmospheric circulation cells associated with the two types of ENSO, we employ three variables: velocity potential, divergent wind, and pressure vertical velocity. Velocity potential and divergent wind, i.e. the Laplacian of velocity potential, are assessed at the atmosphere's upper level (200 hPa). Generally, regions of positive (negative) velocity potential at 200 hPa have converging (diverging) winds and subsidence (ascending motion) beneath. Values of velocity potential at 200 hPa also show information regarding the intensity of atmospheric circulation (Weng et al. 2007). The convergence (divergence) in the upper level corresponds to divergence (convergence) in the lower level (Wang 2002). The descending and ascending regions are specifically illustrated by vertical velocity. Wang (2002) described the vertical velocity's structure associated with the Walker circulation cell across the equatorial Pacific Ocean under EN.

Figure 9a,b shows that the maximum value of velocity potential at 200 hPa for a neutral year is about 15 ($\times 10^6$ m^2 s^{-1}), located in South Atlantic and South Africa during JJA and in North Atlantic and North Africa during DJF. The minimum is observed in the northwestern Pacific and Southeast Asia around 90ºE–170ºE) during JJA and in the western equatorial Pacific during DJF, with a value of -15 ($\times 10^6$ m^2 s^{-1}). The wind at 200 hPa diverges from the location of minimum velocity potential to the place of higher velocity potential, such as the eastern Pacific and Africa. The divergence at the upper level is connected with a strong upward motion associated with the ascending branch of the Walker circulation over the western Pacific, notably over the northwestern Pacific (100ºE-180ºE) in JJA and the western equatorial Pacific (130ºE-140ºW) in DJF (Fig. 11a,b).

Previous studies have shown that differences in the patterns of SSTA in the Pacific Ocean can lead to a shift in the position and intensity of the Walker circulation. For example, under EN in both JJA and DJF, there is a typical positive SSTA in the central and eastern Pacific, and the sea level pressure difference between the East and western Pacific Oceans decreases markedly, leading to a weakening of the Walker circulation (Julian and Chervin 1978; Vecchi et al. 2007; Power and Smith 2007). The equatorial region in the western Pacific Ocean often shows a westerly wind anomaly, due to the weakening of the Walker circulation under EN, in contrast to the easterly anomaly in the eastern Indian Ocean. Thus, this region becomes a divergent zone in the low level under EN (Hosking et al. 2012).

Under EN conditions, the positive values of the composite velocity potential and divergent wind anomalies indicate upper level anomalous convergences (Fig. 9c,d). The upper level anomalous convergence center is located around [110ºE, -20ºS] over the tropical Indian Ocean –a part of the Maritime Continent–Australia region in JJA (Fig. 9c). In DJF, the anomalous center is shifted northeastward to around [120ºE, 0ºN] (Fig. 9d). Conversely, there exist upper level anomalous divergences over the eastern and equatorial central Pacific, where SSTA is positive (Fig. 2). The areas of maximum velocity potential in the eastern Pacific and minimum in the western Pacific are shifted

to West under EN for both JJA and DJF, and the magnitudes decrease to 12 and -10 ($\times 10^6$ $m^2 s^{-1}$), compared to the neutral years' means of ~15 and -15 ($\times 10^6$ m^2 s^{-1}), respectively. These changes correspond to reduced descending motions, due to anomalous warming, in the central and eastern Pacific between 160ºW and 100ºW (120ºW and 80ºW) in JJA (DJF), along with weaker upward motions west of 160ºE (160ºW) in JJA (DJF) (Fig. 11c,d). The weaker upward motions in the ascending branch of the Walker circulation lead to rainfall decrease over the major part of SEA under EN (cf. Fig. 4a,b).

For EM conditions, an upper level anomalous divergence is located over the central Pacific around 180ºW in both seasons, while an anomalous convergence center is found over the southwestern (southeastern) part of SEA in JJA (DJF) (Fig. 9e,f). Compared to EN, the EM convergence and divergence anomalies are generally weaker in terms of magnitude; however the differences are not significant over most of SEA (Fig. 9e,f). The significantly less positive velocity potential anomaly of EM compared to EN over the southeastern part of SEA (15ºN, 150ºE) in JJA (Fig. 9g) and over the southwestern part in DJF (Fig. 9h) indicates stronger upward motions over these areas during EM than EN. These areas belong to the ascending branch of the Walker circulation. The less reduced upward motion in EM compared to EN can be observed between 150ºE and 180ºE (60ºE and 120ºE) in JJA (DJF) (Fig. 11). This explains the significant weaker rainfall deficit in EM compared to EN over the Philippines (R1,2) and Papua (R8) during JJA, and over the southwestern SEA during DJF (cf. Fig. 4e,f).

Our analysis above partly follows that of Weng et al. (2007), who focused on the impacts of EM and EN on rainfall in the Pacific rim (China, Japan and the USA) during boreal summer. The analysis is, however, performed here for the first time over the entire SEA for the recent period 1979–2019, for both boreal summer and winter, and with up-to-date datasets. Moreover, the features during LN and LM, which were not examined in Weng et al. (2007), are presented in the following.

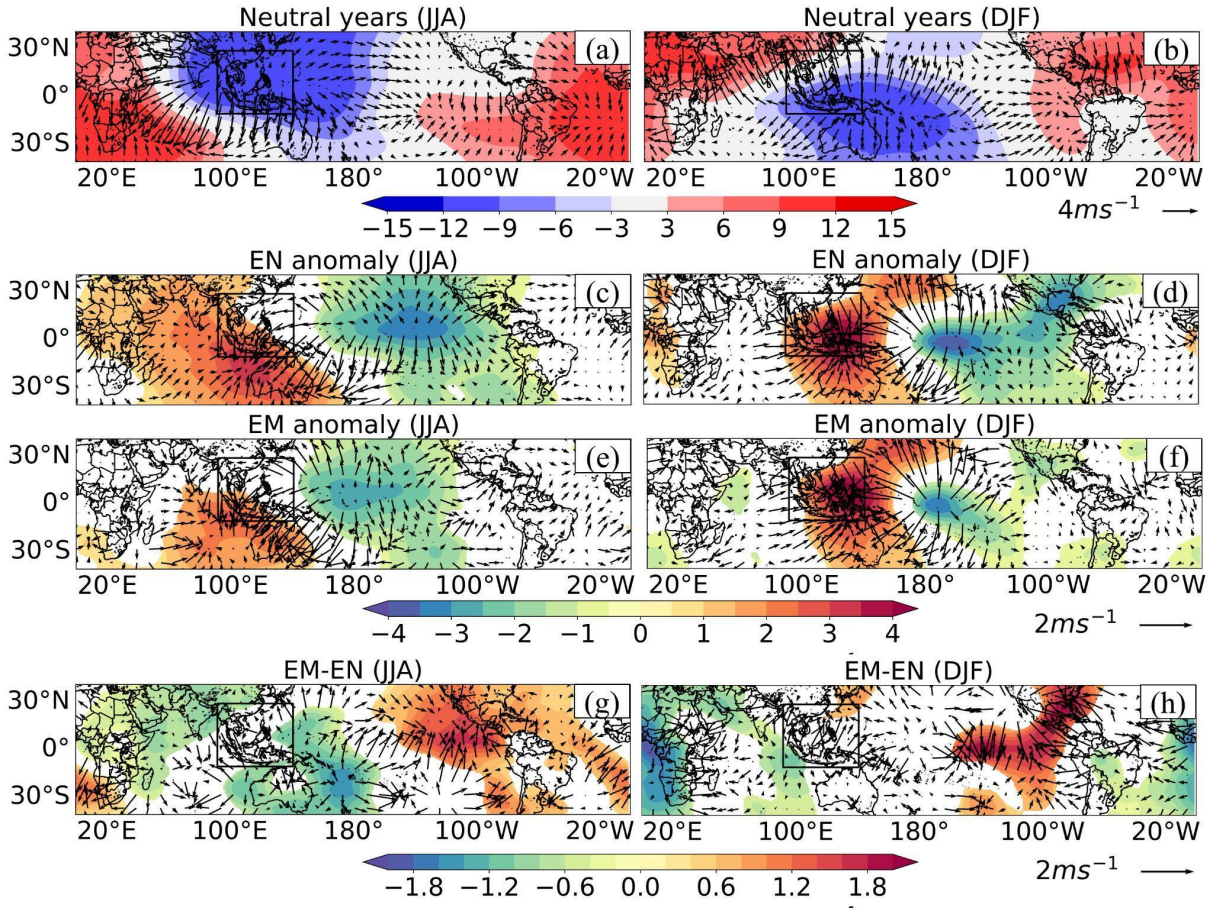

Figure 9. Mean of 200 hPa velocity potential (shading; units: 10^6 m^2s^{-1}) and divergent wind (arrow, unit: ms^{-1}) for the neutral years during (a, b) JJA and DJF. Anomalous velocity potential and divergent wind at the 200 hPa for (c, d) EN and (e, f) EM events and (g, h) the differences between EN and EM anomalies during JJA and DJF. Shading in (c–h) indicates areas where differences are statistically significant at 90% based on the bootstrap test.

The anomalous potential velocity and divergent wind values in LN and LM show opposite patterns compared to those in EN and EM, respectively (Fig. 10). Convergence and divergence are both enhanced compared to the neutral years' means in LM and, to a lesser extent in LN, in both seasons (Fig. 10a–d). In LN, an anomalous divergence at the upper level occurs over the southwest of SEA during JJA and over the entire SEA domain during DJF, corresponding to an intensification of the ascending branch of the Walker circulation over these areas (Fig. 11g,h), hence explaining the increase in rainfall over parts of SEA (cf. Fig. 5a,b). In DJF, there is no significant difference over SEA between LM and LN in terms of potential velocity, divergent wind (Fig. 10f), and

pressure vertical velocity (Fig. 11h,j). In JJA, the difference between LM and LN shows a significant anomalous convergence center at the upper level over the SEA domain (Fig. 10e), corresponding to a reduced upward motion between 100ºE–140ºE (Fig. 11i), thus explaining the weaker rainfall increase or drier conditions over SEA in LM compared to LN (cf. Fig. 5e).

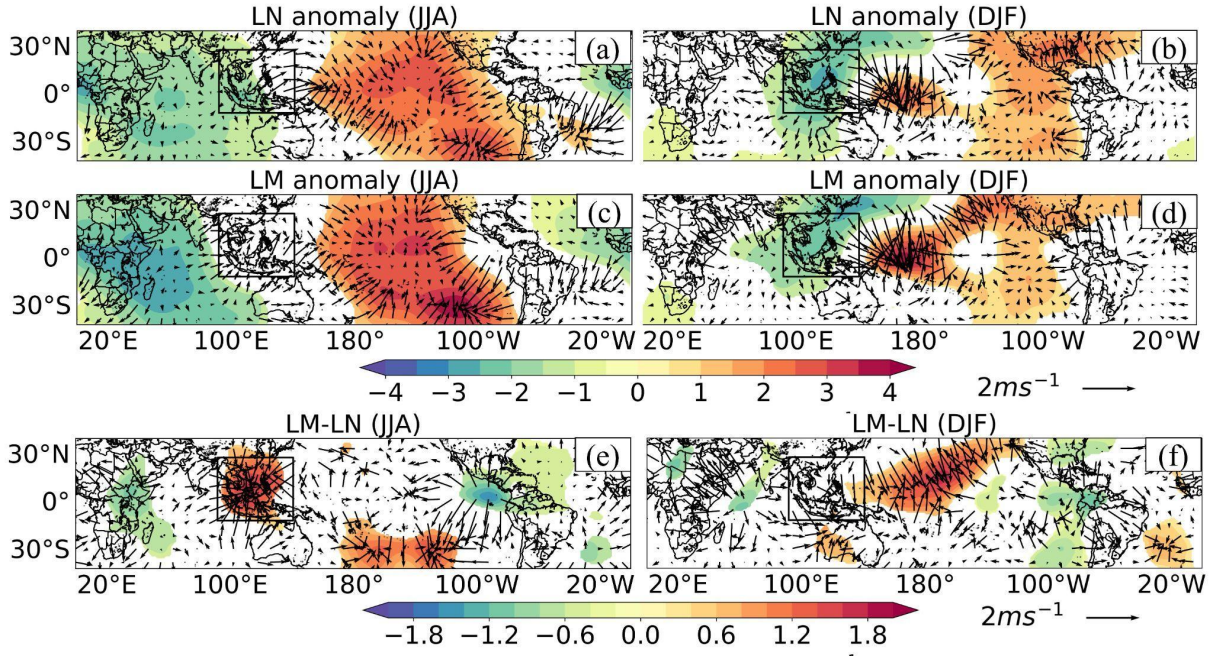

Figure 10. As in Figure 9(c–h) but for LN and LM.

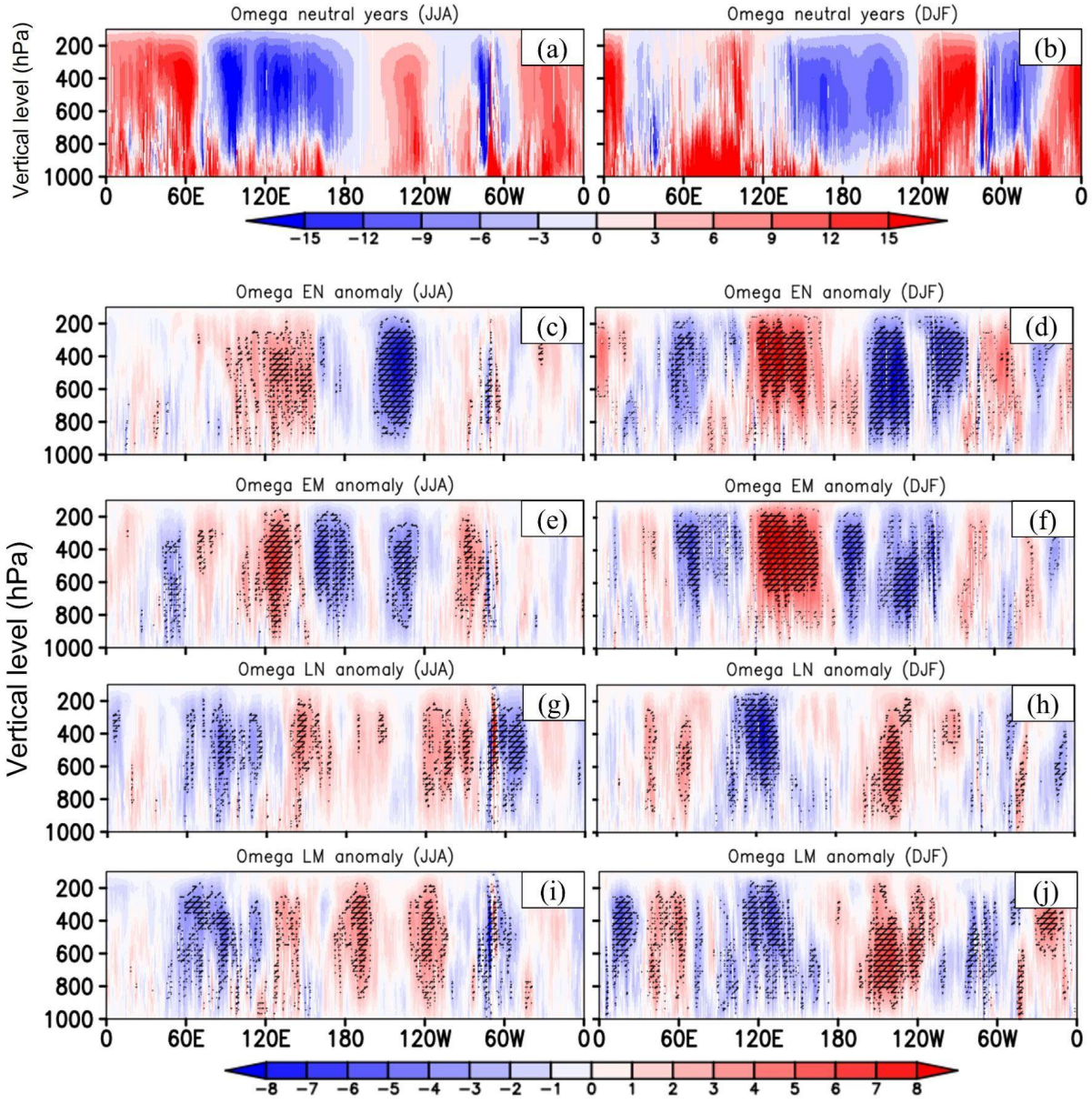

Figure 11. Mean of pressure vertical velocity for the neutral years during (a) JJA and (b) DJF, and composites of pressure vertical velocity anomalies for (c, d) EN, (e, f) EM, (g, h) LN, and (i, j) LM during JJA (left) and DJF (right). The average between 13ºS and 29.5ºN is computed. Units in Pas^{-1}. The hatch patterns in (c–j) indicate areas where differences are statistically significant at 90% based on the bootstrap test.

It is of interest to recognize that the location and strength of the anomalous circulation patterns of each type of ENSO events (Figs. 9–11) correspond to the location and strength of the SSTA maximum (SFig. 4). Previous studies also indicated that atmospheric teleconnections are strongly influenced by different SSTA configurations in the equatorial regions (Capotondi et al. 2015; Abid et al. 2020; Ma et al. 2022). Thus, the differences in the precipitation response between the two types of ENSO events, resulting from the differences in the atmospheric circulations, are linked to the SSTA spatial pattern and intensity. Note that the largest differences in the precipitation response lie in the amplitude rather than the spatial pattern (Figs. 4, 5). These differences appear more likely to be related to the SSTA zonal location during JJA, while the different SSTA amplitudes play a more important role during DJF (Figs. 9–11, and SFig.4).

5 Conclusions

This study depicts, for the first time, the detailed and distinct impacts of ENSO and ENSO Modoki on rainfall over Southeast Asia and its 20 sub-regions during the last 40 years. The EMI and Niño 3 indices were used to identify the Modoki and the classic ENSO events, respectively. Results showed that within the study period of 1979–2019, there were seven EN, six LN events, five EM, and five LM events; and 16 years were classified as neutral years.

Based on the up-to-date GPCC version 2020 dataset at 0.25º resolution, changes in rainfall under ENSO and ENSO Modoki conditions were estimated and associated with the SSTA in the Pacific Ocean and the atmospheric circulation. In JJA under canonical EN conditions, rainfall reduction occurs over most of the southern SEA domain and Southeast Philippines, while alternating drier and wetter conditions occur over Indochina. In DJF of EN events, larger rainfall reduction compared to JJA is seen over Southeast Philippines, East Borneo, and Maluku, while significant rainfall enhancements are observed over West Kalimantan and parts of the Indochinese Peninsula. Similar rainfall anomaly patterns are obtained in EM, though EM shows

enhanced drier/wetter conditions compared to EN. In both EN and EM, the reduction in moisture transport from the Pacific in both JJA and DJF and from the equatorial easterlies in the southern hemisphere in DJF to the SEA region causes a decrease in rainfall over the Maritime Continent in JJA and the northern part of the Maritime Continent and the Philippines in DJF. They are associated with a weakening and westward shift of the ascending and descending branches of the Walker circulation. Under EN, the negative anomalies of the ascending branch of the Walker circulation are located over the southwest and southeast of SEA in JJA and DJF, respectively, thus suppressing rainfall and leading to drier conditions in the region. The negative anomalies of the ascending branch are weaker under EM, resulting in a weaker rainfall reduction compared to EN over the Philippines and Papua during JJA and over the southwestern SEA during DJF.

The impacts of LN and LM on rainfall in Southeast Asia are noticeably different from those of EN and EM. Under LN, rainfall increases in most sub-regions except for West Philippines and some specific locations in Indochina in JJA, and some areas in the southern part of SEA in DJF. Although having the same anomaly patterns, LM generally shows less wet/drier conditions than LN in JJA. In DJF, LM produces more rainfall than LN over most of the Maritime Continents while generally displaying less rainfall over the eastern part of SEA. The LM rainfall deficit compared to LN in JJA comes from a shortage of moisture transport into the north of SEA and from the strong anomalous convergence at the upper level that leads to a weakening of the ascending motion beneath, hence rainfall suppression. Meanwhile, the LM rainfall increase compared to LN in DJF in the southern subregions is attributed to more enhanced moisture transport by the Pacific easterlies and the equatorial westerlies into the region, hence rainfall surplus.

Our results suggest that droughts in EM could be less severe than in EN in almost all subregions during JJA, while floods in LM could be worsened compared to LN in the southern part of SEA during DJF.

We have performed the sensitivity analysis with other rainfall and reanalysis datasets, i.e. the CRU rainfall and the NCEP1 reanalysis datasets. This confirmed the robustness of the obtained results discussed above (not shown). In the present work, the role of heat transfer was not investigated. As latent and sensible heat fluxes were shown to have a close connection with rainfall (Gao et al. 2015; Juneng et al. 2016), the results obtained in this study thus highlight the importance of examining the impacts of both types of ENSO on air-sea heat fluxes across the SEA region. The ability of regional models in reproducing both types of ENSO and their impacts would also deserve to be carefully investigated in a future study.

References

Abid MA et al (2020) Tropical Indian Ocean mediates ENSO influence over Central Southwest Asia during the wet season. Geophys Res Lett 47: e2020GL089308. https://doi.org/10.1029/2020GL089308

Aldrian E, Susanto RD (2003) Identification of three dominant rainfall regions within Indonesia and their relationship to sea surface temperature. Int J Climatol 23:1435−1452

Alsepan G, Minobe S (2020) Relations between interannual variability of regional-scale Indonesian precipitation and large-scale climate modes during 1960–2007. J Clim 33:5271–5291. https://doi.org/10.1175/jcli-d-19-0811.1

An S-I, Wang B (2001) Mechanisms of locking the El Nino and La Nina mature phases to boreal winter. J Clim 14:2164–2176

Ashok K et al (2007) El Niño Modoki and its teleconnection. J Geophys Res 112:C11007. https://doi.org/10.1029/2006JC003798

Bo L, Ren HL (2019) ENSO Features, Dynamics, and Teleconnections to East Asian Climate as Simulated in CAMS-CSM. J Meteorol Res 33:46-65. https://doi.org/10.1007/s13351-019-8101-6

Capotondi A et al (2015) Understanding ENSO Diversity. Bull Ame Meteorol Soc 96(6): 921-938. https://doi.org/10.1175/BAMS-D-13-00117.1

Chen H, Jin F (2020) Fundamental Behavior of ENSO Phase Locking. J Clim 33(5):1953–1968

Chokngamwong R, Chiu LS (2008) Thailand daily rainfall and comparison with TRMM products. J Hydrometeorol 9:256−266

Cruz FT et al (2017) Sensitivity of Temperature to Physical Parameterization Schemes of RegCM4 over the CORDEX-Southeast Asia Region. Int J Climatol 37:5139–5153. https://doi.org/10.1002/joc.5151

D'Arrigo R, Smerdon JE (2008) Tropical climate influences on drought variability over Java, Indonesia. Geophys Res Lett 35: L05707. https://doi.org/10.1029/2007GL032589

Deser C, Guo R, Lehner F (2017) The relative contributions of tropical Pacific sea surface temperatures and atmospheric internal variability to the recent global warming hiatus. Geophys Res Lett 44:7945–7954. https://doi.org/10.1002/2017gl074273

Efron B and Tibshirani R J (1993) An Introduction to the Bootstrap. New York: Chapman &Hall, 436pp.

Fasullo J, Webster PJ (2003) A hydrological definition of Indian Monsoon onset and withdrawal. J Clim 16:3200–3211. https://doi.org/10.1175/1520-0442

Feng J et al (2010) Different impacts of two types of Pacific Ocean warming on Southeast Asian rainfall during boreal winter. J Geophys Res 115:D24122. https://doi.org/10.1029/2010JD014761

Feng S, Hu Q (2004) Variations in the teleconnection of ENSO and summer rainfall in northern China: A role of the Indian summer monsoon. J Clim 17:4871–4881. https://doi.org/10.1175/JCLI-3245.1

Francisco RV et al (2006) Regional model simulation of summer rainfall over the Philippines: effect of choice of driving fields and ocean flux schemes. Theor Appl Climatol 86:215−227

Gao Y et al (2015) Assessing and improving noah-MP land model simulations for the central Tibetan plateau. J Geophys Res Atmos 120:9258-9278, https://doi.org/10.1002/2015JD023404

Harger JRE (1995) Air-temperature variations and ENSO effects in Indonesia, the Philippines, and El Salvador: ENSO patterns and changes from 1866–1993. Atmos Environ 29:1919–1942

Harris I, Osborn T J, Jones P, Lister D (2020). Version 4 of the CRU TS monthly high-resolution gridded multivariate climate dataset. Sci Data, 7(1), 109–. https://doi:10.1038/s41597-020-0453-3

Helmholtz H (1867) On Integrals of the hydrodynamical equations, which express vortex-motion. The London, Edinburgh, and Dublin Philosophical Magazine and J Science 33(226): 485–512. https://doi.org/10.1080/14786446708639824

Hendon HH (2003) Indonesia rainfall variability: Impacts of ENSO and local air-sea interaction. J Clim 16:1775–1790

Hendrawan IG, Asai K, Triwahyuni A, Lestari DV (2019) The interannual rainfall variability in Indonesia corresponding to El Niño Southern Oscillation and Indian Ocean Dipole. Acta Oceanologica Sinica 38(7):57–66. https://doi.org/10.1007/s13131-019-1457-1

Hersbach H, Bell B, Berrisford P, et al. (2020) The ERA5 global reanalysis. Q J R Meteorol Soc. 146: 1999– 2049. https://doi.org/10.1002/qj.3803

Hosking JS et al. (2012). Tropical convective transport and the Walker circulation. Atmos Chem Phys 12:9791–9797. http://doi.org/10.5194/acp-12-9791-2012

Huang P, Xie S (2015) Mechanisms of change in ENSO-induced tropical Pacific rainfall variability in a warming climate. Nat Geosci 8(12):922–926. https://doi.org/10.1038/ngeo2571

Julian R, Chervin RM (1978) A Study of the Southern Oscillation and Walker Circulation Phenomenon. Mon Weather Rev 106(10):1433–1451. https://doi.org/10.1175/1520-0493(1978)106<1433:asotso>2.0.co;2

Juneng L, Tangang FT (2005) Evolution of ENSO-related rainfall anomalies in Southeast Asia region and its relationship with atmosphere–ocean variations in Indo-Pacific sector. Clim Dyn 25:337–350. https://doi.org/10.1007/s00382-005-0031-6

Juneng L et al (2007) Simulation of tropical cyclone Vamei (2001) using the PSU/NCAR MM5 model. Meteorol Atmos Phys. 97:273−290

Juneng L et al (2016) Sensitivity of the Southeast Asia Rainfall Simulations to Cumulus and Ocean Flux Parameterization in RegCM4. Clim Res 69:59-77. https://doi.org/10.3354/cr01386

Kalnay E et al (1996) The NCEP/NCAR 40-year reanalysis project. Bull Am Meteorol Soc 77:437–440

Kao HY, Yu JY (2009) Contrasting Eastern-Pacific and Central-Pacific Types of ENSO. J Clim 22(3):615–632. https://doi.org/10.1175/2008jcli2309.1

Karori MA, Li J, Jin F (2013) The Asymmetric Influence of the Two Types of El Niño and La Niña on Summer Rainfall over Southeast China. J Clim 26(13):4567–4582. https://doi.org/10.1175/jcli-d-12-00324.1

Kug J S, Jin FF, An SI (2009) Two Types of El Niño Events: Cold Tongue El Niño and Warm Pool El Niño. J Clim 22(6):1499–1515. https://doi.org/10.1175/2008jcli2624.1

Larkin NK, Harrison DE (2005) Global seasonal temperature and precipitation anomalies during El Niño autumn and winter. Geophys Res Lett 32: L13705. https://doi.org/10.1029/ 2005GL022738

Lestari S et al (2016) ENSO Influences on Rainfall Extremes around Sulawesi and Maluku Islands in the Eastern Indonesian Maritime Continent. SOLA 12(0):37–41. https://doi.org/10.2151/sola.2016-008

Li LM et al (2011) The recycling rate of atmospheric moisture over the past two decades (1988-2009). Environ Res Lett 6:034018. https://doi.org/10.1088/1748-9326/6/3/034018

Ma T et al (2022) Different ENSO Teleconnections over East Asia in Early and Late Winter: Role of Precipitation Anomalies in the Tropical Indian Ocean and Far

Western Pacific. J Clim 35(24): 4319-4335. https://doi.org/10.1175/JCLI-D-21-0805.1

Marathe S, Ashok K, Swapna P, Sabin TP (2015) Revisiting El Niño Modokis. Clim Dyn 45:3527–3545. https://doi.org/10.1007/s00382-015-2555-8

Matsumoto J (1997) Seasonal transition of summer rainy season over Indochina and adjacent monsoon region. Adv Atmos Sci 14:231–245

McPhaden MJ, Zebiak SE, Glantz MH (2006) ENSO as an Integrating Concept in Earth Science. Science 314(5806):1740–1745. https://doi.org/10.1126/science.1132588

Nguyen-Thi HA, Matsumoto J, Ngo-Duc T, Endo N (2012) A climatological study of tropical cyclone rainfall in Viet- nam. SOLA 8:41−44

NOAA-CPC (2022) https://origin.cpc.ncep.noaa.gov/products/analysis_monitoring/ensostuff/ONI_v5.php (last accessed in June 2022)

Page SE et al (2002) The amount of carbon released during peat and forest fires in Indonesia during 1997. Nature 420:61–65

Phan VT, Ngo-Duc T, Ho TMH (2009) Seasonal and interannual variations of surface climate elements over Vietnam. Clim Res 40: 49-60

Power SB, Smith IN (2007) Weakening of the Walker Circulation and apparent dominance of El Niño both reach record levels, but has ENSO really changed? Geophys Res Lett 34(18):L18702. https://doi.org/10.1029/2007gl030854

Räsänen TA et al (2016) On the spatial and temporal variability of ENSO precipitation and drought teleconnection in mainland Southeast Asia. Clim Past 12:1889–1905. https://doi.org/10.5194/cp-12-1889-2016

Rasmusson EM, Wallace JM (1982) Meteorological aspects of the El Niño/Southern Oscillation. Science 222(4629):1195– 1202.

Rasmusson EM, Carpenter TH (1983) The relationship between Eastern equatorial Pacifc sea surface temperatures and rainfall over India and Sri Lanka. Mon Weather Rev 111:517–528

Rayner NA et al (2003) Global analyses of SST, sea ice and night marine air temperature since the late nineteenth century. J Geophys Res 108:. https://doi.org/10.1029/2002JD002670

Rudolf B, Hauschild H, Reuth W, Schneider U (1994) Terrestrial precipitation analysis: Operational method and required density of point measurements. Global Precipitation and Climate Change (M. Desbois, F. Desalmond, eds.), NATO ASI Series I, 26:173-186

Salimun E et al (2013) Differential impacts of conventional El Niño versus El Niño Modoki on Malaysian rainfall anomaly during winter monsoon. Int J Climatol 34(8):2763–2774. https://doi.org/10.1002/joc.3873

Saji N, Goswami B, Vinayachandran P, Yamagata T (1999) A dipole mode in the tropical Indian Ocean. Nature 401:360–363.

Shinoda T, Hurlburt HE, Metzger EJ (2011) Anomalous tropical ocean circulation associated with La Niña Modoki. J Geophys Res Atmos 116:C12001. https://doi.org/10.1029/2011JC007304

Shukla RP, Tripathi KC, Pandey AC, Das IML (2011) Prediction of Indian summer monsoon rainfall using Niño indices: A neural network approach. Atmos Res 102(1-2):99–109. https://doi.org/10.1016/j.atmosres.2011.06.013

Tangang FT et all (2017) Characteristics of precipitation extremes in Malaysia associated with El Niño and La Niña events. International Journal of Climatology. https://doi:10.1002/joc.5032

Tangang FT et al (2020) Projected Future Changes in Rainfall in Southeast Asia based on CORDEX–SEA multi-model simulations. Clim Dyn 55(5):1247-1267. https://doi.org/10.1007/s00382-020-05322-2

Timmermann A et al (2018) El Niño–Southern Oscillation complexity. Nature 559:535–545. https://doi.org/10.1038/s41586-018-0252-6

Trenberth KE (1997) The Definition of El Niño. Bull Amer Meteorol Soc 78(12):2771–2777. https://doi.org/10.1175/1520-0477(1997)078<2771:tdoeno>2.0.co;2

Trenberth KE et al (1998). Progress during TOGA in understanding and modeling global teleconnections associated with tropical sea surface temperatures. J Geophys Res 103(C7):14291–14324. http://doi.org/10.1029/97JC01444

Vecchi GA et al (2006) Weakening of tropical Pacific atmospheric circulation due to anthropogenic forcing. Nature 441: 73-76

Wang B, Wu R, Fu X (2000) Pacific –East Asian teleconnection: how does ENSO affect East Asian climate. J Clim 13:1517–1536

Wang C (2002) Atmospheric circulation cells associated with the El Nino Southern Oscillation. J Clim 15:399–419

Wang W, Chen M, Kumar A, Xue Y (2011) How important is intraseasonal surface wind variability to real-time ENSO prediction? Geophys Res Lett 38(13). https://doi.org/10.1029/2011gl047684

Webster P, Moore A, Ioschnigg J, Leben R (1999) Coupled ocean-atmosphere dynamics in the Indian Ocean during 1997–1998. Nature 401:356–360

Weng H et al (2007) Impacts of recent El Niño Modoki on dry/wet conditions in the Pacific rim during boreal summer. Clim Dyn 29(2-3):113–129. https://doi.org/10.1007/s00382-007-0234-0

Weng S, Behera K and Yamagata T (2009) Anomalous winter climate conditions in the Pacific rim during recent El Niño Modoki and El Niño events. Clim Dyn. 32:663–674. https://doi.org/10.1007/s00382-008-0394-6

Wu R, Hu ZZ, Kirtman BP (2003) Evolution of ENSO-related rainfall anomalies in East Asia and the processes. J Clim 16: 3742–3758

Zhou TJ, Yu RC (2005) Atmospheric water vapor trans-port associated with typical anomalous summer rainfall patterns in China. J Geophys Res 110:D08104. https://doi.org/10.1029/2004JD005413

Xu K et al (2017) CMIP5 Projections of Two Types of El Niño and Their Related Tropical Precipitation in the Twenty-First Century. J Clim 30(3):849–864. https://doi.org/10.1175/jcli-d-16-0413.1

Xue F, Liu CZ (2008) The influence of moderate ENSO on summer rainfall in eastern China and its comparison with strong ENSO (in Chinese). Chin Sci Bull 53(5):791–800. https://doi.org/10.1007/s11434-008-0002-5

Yan J et al (2020) Temporal Convolutional Networks for the Advance Prediction of ENSO. Sci Rep 10:8055. https://doi.org/10.1038/s41598-020-65070-5

Yeh SW et al (2009) El Niño in a changing climate. Nature 461:511–514

Yu JY, Kao HY (2007) Decadal changes of ENSO persistence barrier in SST and ocean heat content indices: 1958–2001. J Geophys Res 112:D13106. https://doi.org/10.1029/2006JD007654

Yu JY, Zou Y, Kim ST, Lee T (2012) The changing impact of El Niño on US winter temperatures. Geophys Res Lett 39: L15702. https://doi.org/10.1029/2012GL052483

Yu JY, Zou Y (2013) The enhanced drying effect of central-Pacific El Niño on US winter. Environ Res Lett 8:014019. https://doi.org/10.1088/1748-9326/8/1/014019

Statements & Declarations

Funding

This study was supported by the LOTUS international joint laboratory (lotus.usth.edu.vn) funded by IRD and the Vietnam National Foundation for Science and Technology Development (NAFOSTED). Hue Nguyen-Thanh's Ph.D. thesis is supported by the French Embassy in Vietnam via the scholarship of Excellence.

Competing interests

The authors have no conflicts of interest to declare.

Author Contributions

All authors contributed to the writing of the manuscript. Hue Nguyen-Thanh produced figures, processed data, and prepared an initial draft. Thanh Ngo-Duc and Marine Herrmann supervised the overall work. The study was conceptualized by Thanh Ngo-Duc.

Data Availability

Data sharing is not applicable to this article as no datasets were generated.

Ethical Approval

Ethical approval is not applicable to this article.

Supplemental Tables

Supplemental Table 1. List of ENSO and ENSO Modoki months over the period of 1979–2019. Results are obtained with the Niño3 index. Slightly different results obtained with the Niño3.4 index are indicated in the parentheses. The last row shows the total number of months for each event.

El Niño	El Niño Modoki	La Niña	La Niña Modoki
04(05)/1982–06(05)/1983			
			09/1983–05/1984
		10(09)/1984–08/1985	
09/1986–11/1987(01/1988)			
		04(05)/1988–10/1988	11/1988–05/1989
	08/1991–02/1992		
	05/1994–05/1995		
		08(09)/1995–03(02)/1996	
05/1997–05/1998			06/1998–05/1999
		06/1999–03(05)/2000	
	07/2002–03/2003		
	06/2004–03/2005		
09/2006–01/2007			
		07/2007–12/2007	01/2008–03/2009
	10/2009–03/2010		
		06/2010–05/2011	
			10/2011–03/2012
11/2014–04/2016			

		10(09)/2017–04(03)/2018	
	06/2018–10/2018		
11/2018–06/2019			
	07/2019–12/2019		
74 (74)	**56 (56)**	**61 (61)**	**49 (49) (months)**

Supplemental Figures

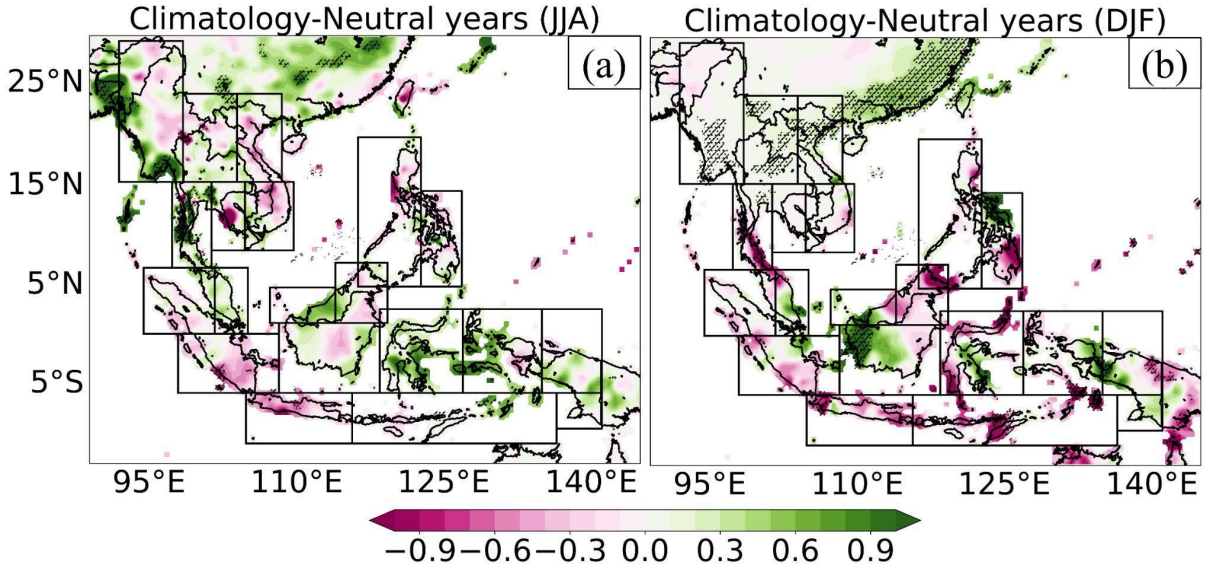

SFig. 1. Differences between climatology and neutral values for (a) JJA and (b) DJF. Units in mm/day. The dot pattern indicates areas where differences are statistically significant at 90% based on the Student's t-test.

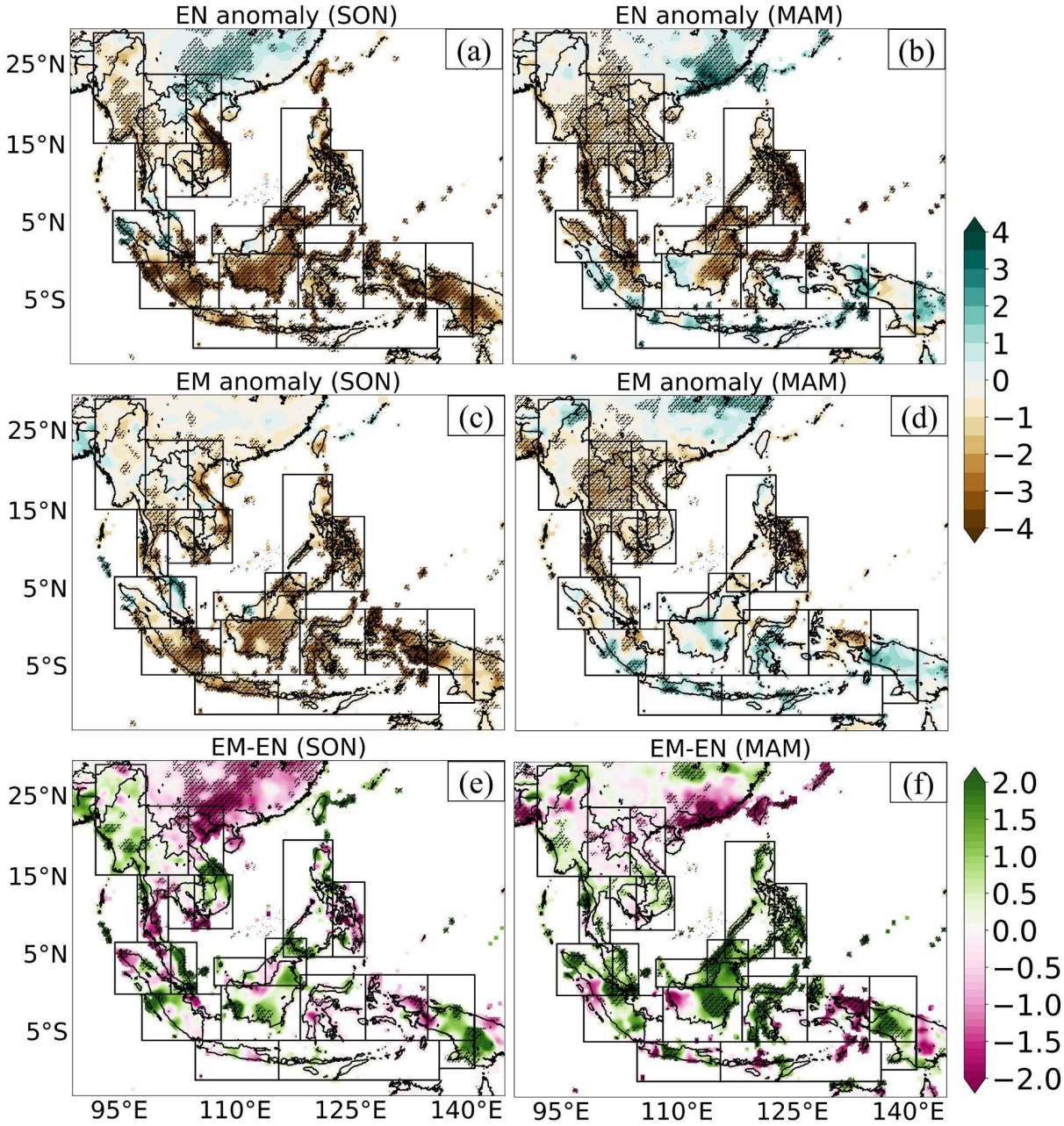

SFig. 2. Composites of SON and MAM rainfall anomalies (units: mm/day) for (a, b) EN, (c, d) EM, and (e, f) the differences between EN and EM. The dot pattern indicates areas where differences are statistically significant at 90% based on the bootstrap test.

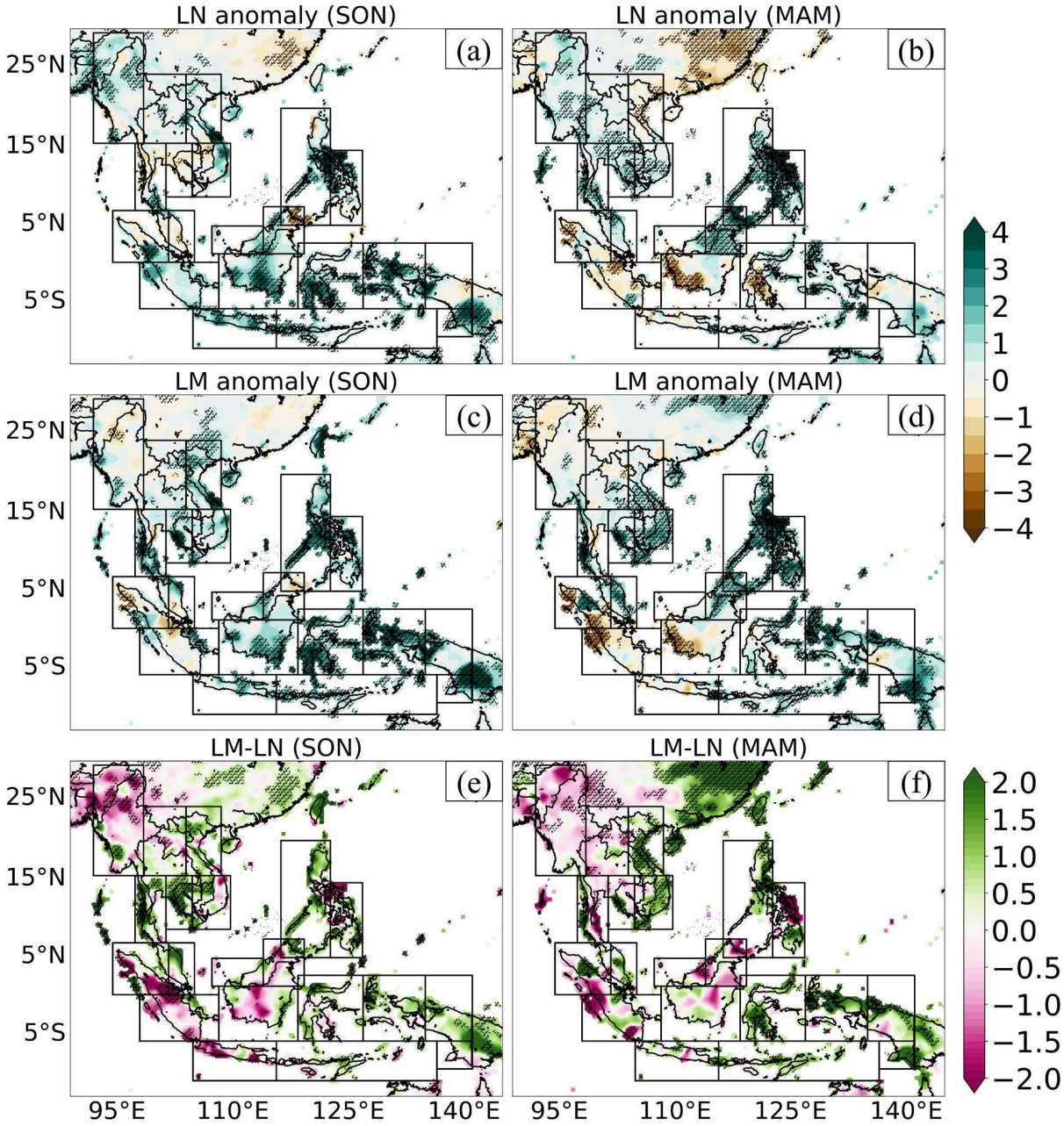

SFig. 3. As in SFig. 2 but for LN and LM.

s

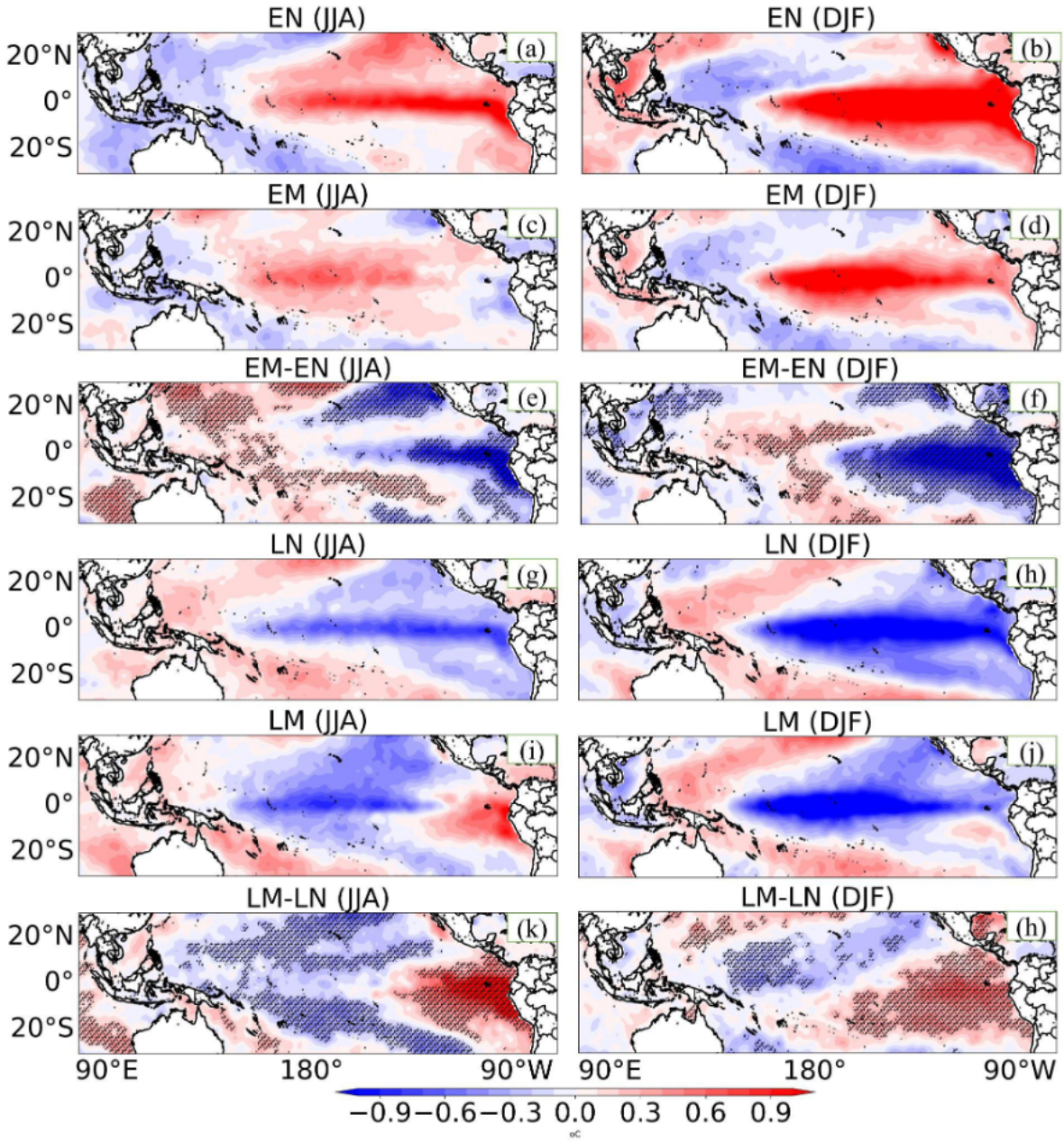

SFig. 4. Composites of JJA and DJF sea surface temperature anomalies (SSTA) (units: ℃) for (a, b) EN, (c, d) EM, and (e, f) the differences between EN and EM; (g, h) LN, (i, j) LM, and (k, h) the differences between LN and LM. The dot pattern indicates areas where differences are statistically significant at 90% based on the bootstrap test.